

XROTOR

X-shaped Radical Offshore Wind Turbine for Overall Cost of Energy Reduction

D5.1

Secondary rotors and powertrain design

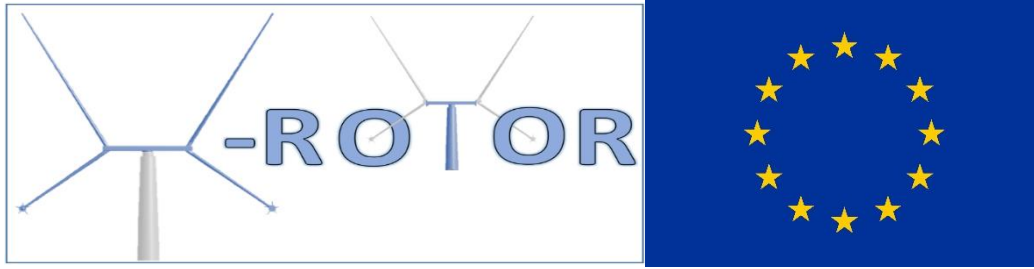
 <https://xrotor-project.eu>

 @XROTORProject

December 2021



This project has received funding from the European Union's Horizon 2020 research and innovation programme under grant agreement No 101007135



X-SHAPED RADICAL OFFSHORE WIND TURBINE FOR OVERALL COST OF ENERGY REDUCTION

Project acronym: **XROTOR**
 Grant agreement number: 101007135
 Start date: 01st January 2021
 Duration: 3 years

WP5 Power take-off and conversion system design T5.2 –Generator and power converters **D5.1 Secondary rotors and power train design**

Lead Beneficiary: University of Strathclyde
 Delivery date: 20 December 2021

Author(s) information (alphabetical):

Name	Organisation	Email
David Campos-Gaona	University of Strathclyde	d.campos-gaona@strath.ac.uk
Adam Stock	University of Strathclyde	adam.stock@strath.ac.uk
William Leithead	University of Strathclyde	w.leithead@strath.ac.uk
Olimpo Anaya-Lara	University of Strathclyde	olimpo.anaya-lara@strath.ac.uk
Laurence Morgan	University of Strathclyde	laurence.morgan@strath.ac.uk

Document Information

Version	Date	Description	Prepared by	Reviewed by	Approved by
1	21/12/2021	Final version	All authors above	W. Leithead & J. Carroll	W. Leithead <i>W. Leithead</i> (Project Coordinator)



The XROTOR Project has received funding from the European Union’s Horizon 2020 research and innovation programme under grant agreement no. 101007135. For more information on the project, its partners, and contributors please see <https://XROTOR-project.eu>.

Executive Summary

Deliverable Description:

Deliverable 5.1 reviews the aerodynamic design constraints of the X-Rotor secondary rotors in terms of tip speed, rotational speed, rated power, dimensions as well as operational strategies. It also provides a generator and a power converter design strategy/framework to address the particular features of the secondary rotor power take-off from an electrical, electromagnetic and construction perspective. The characteristics of the aerodynamics, operational strategies and generators need to be consistent.

This deliverable starts by reviewing the X-rotor operational strategy and identifying the requirements needed from the generators and power electronic control systems. Conventional type-IV wind turbines are compared against the secondary rotor requirements, and a design strategy is proposed to modify standard type-IV designs within realistic design specifications, desired efficiencies, size and cost. Such a design strategy implies the solution of a multi-parameter problem. Most of the design variables of permanent magnet synchronous machines are involved (e.g., volume, length, diameter, PM size, windings, air gap and many others). To obtain an optimal solution, metaheuristic algorithms using real-world design specifications and constraints are applied.

The solutions provided by the design strategy are validated using an Electromagnetic field solver where the elements, dimensions and characteristics of the optimised generator are reproduced in 2-D models. The electrical and electromagnetic performances are corroborated using finite element analysis.

Finally, the electric features of the optimised generator design are used to create an electromagnetic simulation environment where the interaction of the generator and power electronics is revised. In this stage, the minimum requirements of power electronic converters are specified for the range of operating speeds of the secondary rotors. This section also reviews the implications in efficiency and practicality of the minimum requirements of power electronic converters needed.

Responsible:

This deliverable was prepared at the University of Strathclyde by a research team under the guidance of Professor Olimpo Anaya-Lara.

Outcome Summary:

The results presented in this report include a detailed analysis of the optimal design of PMSG for the X-rotor, seeking to comply with the operation strategy of the system, structural limitations and operational ranges. The results of this deliverable include up-to-date information of industrial practices for the development and control of PMSG for wind turbine applications.

The report applies an authoritative design methodology aided by an optimization algorithm and real manufacture constraints to develop an optimal design for a 690V and 3.3KV PMSG machines, since both options could be suitable for the X-rotor system. The results of the design are corroborated and provided as design parameters.

Finally, the report analyses the electric performance of the designed machines under operation conditions that mimic the most extreme operation strategies of the X-rotor. This analysis is used to assess the adequacy of commercial power converters to exert control under those conditions. Clear limits are identified and presented to the designers for each generator design case.

The evaluation of all the material presented in this report suggest that using Medium Voltage PMSG (3.3KV) controlled by 3-level Power Electronic converters with extended DC voltage bus, are the most suitable option for drivetrain design, fulfilling the requirements in size, efficiency, PM usage and operative regimes of the X-rotor concept.

Contents

1. Deliverable Details	3
------------------------------	---

2. Revision of the X-rotor operational strategy.....	4
3. Defining the rotor speed, ratings and dimension of the secondary rotors	8
Aerodynamic Factors.....	8
O&M, Parasitic Drag and Environmental Factors.....	10
Primary Rotor Led Design	10
4. Initial assessment of PMSG requirements.....	11
Concluding remarks.....	14
5. PMSG generator design using heuristic methods	14
PMSG design strategies and considerations.....	14
PMSG design exercise using genetic algorithms	20
Optimization Results for the 3.3KV generator	23
Optimization Results for the 690V generator	26
6. PMSG generator design validation using electromagnetic field solvers.....	30
3.3KV PMSG	30
690V PMSG.....	33
7. Analysis of power electronic requirements using electrical modelling and simulations.....	36
Electrical simulation results of the 690V PMSG	37
Electrical simulation results of the 3.3KV PMSG.....	38
8. Summary of deliverable outcomes.....	40
9. Conclusions.....	40
10. References.....	40

1. Deliverable Details

Deliverable 5.1 reviews the aerodynamic design constraints of the X-Rotor secondary rotors in terms of tip speed, rotational speed, rated power, dimensions as well as operational strategies. It also provides a generator and a power converter design strategy/framework to address the particular features of the

secondary rotor power take-off from an electrical, electromagnetic and construction perspective. The characteristics of the aerodynamics, operational strategies and generators need to be consistent.

The framework uses the widely used type-IV wind turbine generators (i.e. Permanent magnet Synchronous Generators, PMSG, with fully rated converters) as a starting point and analyses the design and specification requirements to achieve the desired efficiencies, size and performance over the unconventional operating speeds and torque provision of the secondary rotors. Particular care ensures that realistic generator and power converter designs are attained by using real-world design specifications and constraints in each case.

This deliverable starts by reviewing the X-rotor operational strategy and identifying the requirements needed from the generators and power electronic control systems. Conventional type-IV wind turbines are compared against the secondary rotor requirements, and a design strategy is proposed to modify standard type-IV designs within realistic design specifications, desired efficiencies, size and cost. Such a design strategy implies the solution of a multi-parameter problem. Most of the design variables of permanent magnet synchronous machines are involved (e.g., volume, length, diameter, PM size, windings, air gap and many others). To obtain an optimal solution, metaheuristic algorithms using real-world design specifications and constraints are applied.

The solutions provided by the design strategy are validated using Maxwell-Ansys Electromagnetic field solver where the elements, dimensions and characteristics of the optimised generator are reproduced in 2-D models. The electrical, electromagnetic and thermal performances are corroborated using finite element analysis.

Finally, the electric features of the optimised generator design are used to create an electromagnetic simulation environment where the interaction of the generator and power electronics is revised. In this stage, the minimum requirements of power electronic converters are specified for the range of operating speeds of the secondary rotors (e.g., power rating, DC voltage, reactive power control capabilities). Additionally, this section analyses the implications in terms of efficiency and practicality of the minimum requirements of power electronic converters needed. The conclusions of this section are helpful to adjust the desired limits of operation of the secondary rotors for a more realistic and close to market design.

The results presented in this report include a detailed analysis of the optimal design of PMSG for the X-rotor seeking to comply with the operation strategy of the system, structural limitations and operational ranges. The results of this deliverable include up-to-date information of industrial practices for the development and control of PMSG for wind turbine applications.

The report applies an authoritative design methodology aided by an optimization algorithm and real manufacture constraints to develop an optimal design for a 690V and 3.3KV PMSG machines, since both options could be suitable for the X-rotor system. The results of the design are corroborated and provided as design parameters.

Finally, the report analyses the electric performance of the designed machines under operation conditions that mimic the most extreme operation strategies of the X-rotor. This analysis is used to assess the adequacy of commercial power converters to exert control under those conditions. Clear limits are identified and presented to the designers for each generator design case

2. Revision of the X-rotor operational strategy

The operational strategy of the X-rotor may be regarded as similar to that of a variable speed pitch regulated HAWT. However there are some aspects of the X-rotor concept that are somewhat different:

1. The aerodynamic torque on the primary rotor is not balanced by the reaction torque from a generator. Instead, it is balanced by the thrust on the secondary rotors. As such, the energy conversion is carried out entirely by the generators at the secondary rotors.
2. In below-rated operation, the turbine is regulated by changing the frequency on the power connection to the secondary rotor, thereby, changing their rotational speed and thrust. Having the primary rotor operating at its λ_{max} induces a wind speed on the secondary rotor that increases linearly with the rotational speed of the primary rotor. Having the secondary rotor, also tracking its λ_{max} , causes the ratio of the thrust on the secondary rotors to the primary rotor torque to be constant irrespective of wind speed. In constant wind speed, both the thrust on the secondary rotors and the primary rotor torque are constant. These equilibrium operating points are stable. In the event of a misbalance due to errors in the assumed aerodynamic characteristics, the states would adjust themselves to find more appropriate equilibrium operating points. In below rated operation, neither the primary nor secondary rotors would now track their C_{pmax} . However, the λ of the rotors would still remain close to λ_{max} .
3. The relationship of aerodynamic torque on the primary rotor to pitch angle is somewhat different to conventional HAWT. The aerodynamics of the primary rotor are shown in Figure 1 a) and b), namely, its C_p - λ curve and pitch schedule to maintain constant torque at constant rotor speed in above rated conditions. The value of λ_{max} is in line with expectations for that of a two-blade HAWT with a slighter higher value of C_{pmax} that still requires validation. As seen in Figure 1 b) the pitching schedule assumes that the primary rotor operates at C_{pmax} up to rated wind speed, at which point pitching commences. As seen in the figure, an initial rapid change in pitch angle is required over a narrow wind speed range followed by a relatively slow change. In this pitching schedule, the pitch angles are negative; that is, during the upstream sweep, the blades are pitched away from feather.

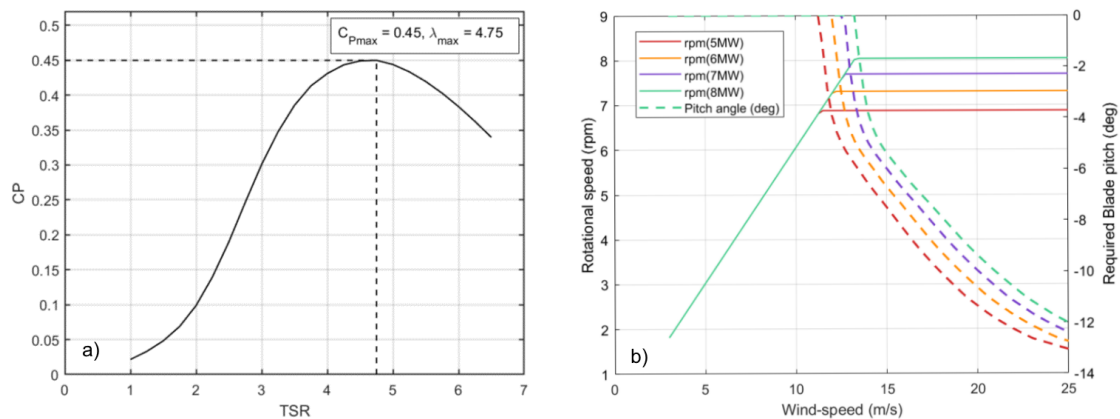


Figure 1 Aerodynamics of the primary rotor[1]. a) C_p - λ curve b) Pitching schedule

Contour plots for C_p on the λ /pitch angle plane are shown in Figure 2. With a fixed positive offset in pitch angle, the value of C_{pmax} increases to greater than 0.52. This is too optimistic but it does indicate that a higher value of C_{pmax} can be achieved in this way, even to values similar to those of a HAWT. Two possible pitching strategies for above-rated conditions are possible, negative pitching or positive pitching. These are shown in Figure 3.

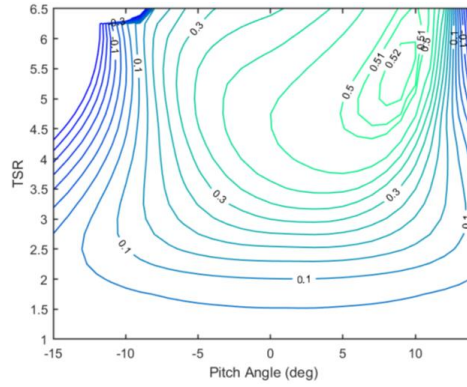


Figure 2 C_p contours on λ -pitch plane of the primary rotor[1]

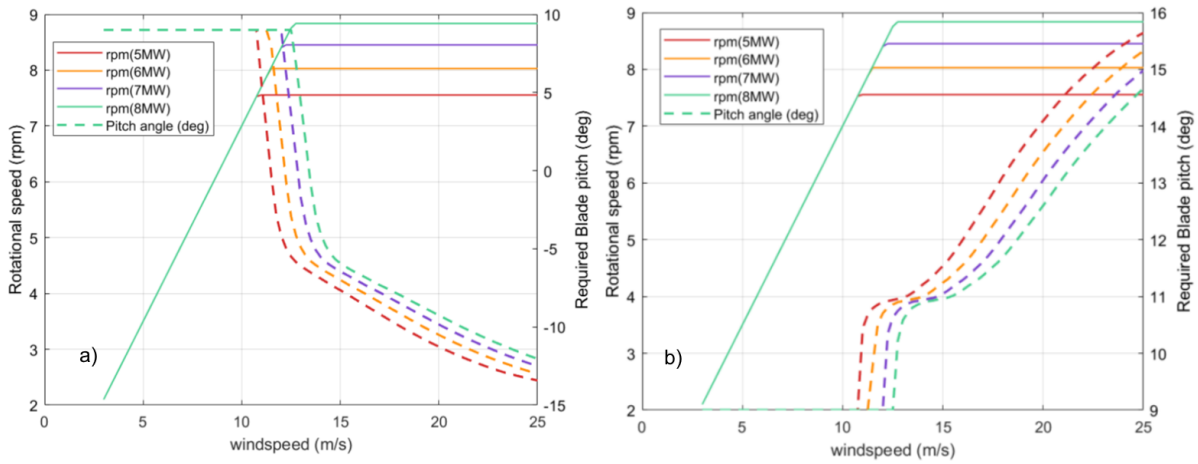


Figure 3 Aerodynamics of the primary rotor [1]. a) Negative pitching strategy b) Positive pitching strategy

The negative pitching strategy is depicted in Figure 3 a). The initial positive offset has to be unwound during the transition to above rated, thereby, greatly increasing the duration of the initial rapid change in pitch. The positive pitching strategy, wherein the blades are pitched towards feather on the upstream sweep, is depicted in Figure 3 b). The requirement for the initial rapid change in pitch angle is similar to the case with no fixed positive pitch offset. The thrust on the primary rotor is shown in Figure 4 for the different pitching strategies.

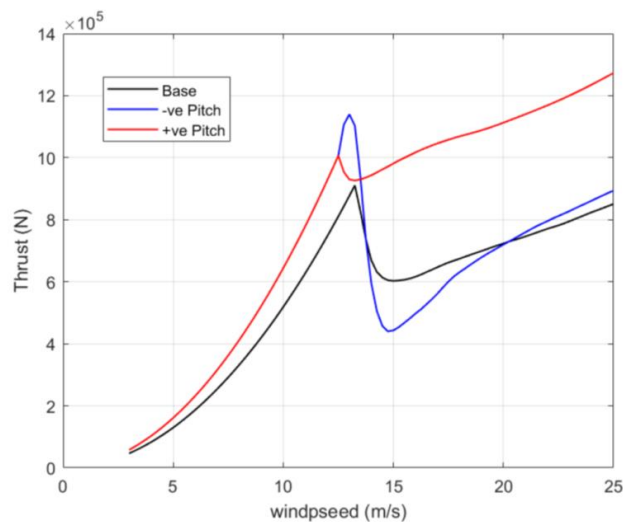


Figure 4 Thrust on the primary rotor [1]

4. In constant wind speed, each secondary rotor experiences a sinusoidal varying wind speed as it rotates going periodically into and out of the ambient wind speed. By operating each secondary rotor to maintain a constant tip speed ratio as it rotates, the energy capture is increased by approximately $100(V_w/V_i)^2\%$ where V_w is the ambient wind speed and V_i is the wind speed induced by the rotation of the primary rotor. Operating in this manner does not appreciably increase loading on the primary rotor or support structure of the turbine. In below rated wind speed, this increase is roughly about 4% but in above rated wind speed it increases rapidly to about 16% at a wind speed of 20m/s. The amplitude of the associated oscillation in the rotational speed of the secondary rotor is about 10% of its mean rotational speed at 5m/s, 20% at 10m/s and 40% at 20m/s. Due to the very low inertia of the secondary rotors and the low rotational speed of the primary rotor, 8RPM at rated wind speed, these periodic variation in the rotational speed of the secondary rotors are easily achieved in lower wind speeds. However, it might become more challenging to do so in wind speeds greatly above rated.

The choice of control strategy for the turbine depends strongly on the above differences from the HAWT case.

The maximum tip-speed for the secondary rotors has three contributing factors. Given that rated wind speed needs to be kept at a value typical of today's turbines, the greater is the product of the two tip speed ratios then the higher is the tip speed of the secondary rotors. Hence, introducing the fixed offset in pitch discussed in point 3 would increase the maximum tip speed by about 16%. In addition, fully utilising in all wind speeds the azimuthal variation in rotational speed discussed in point 4 would increase the maximum tip speed by at least a further 40%. Given that the nominal maximum tip speed, with no fixed offset in pitch and no azimuthal variation in rotational speed, is slightly lower than half the speed of sound, the resulting maximum tip speed would be unacceptable. To address this issue, two options are considered as follows:

The first option is to combine fixed-pitch offset with a reduced utilisation of azimuthal variation in rotational speed of the secondary rotors. With a fixed-pitch offset of 9° , the primary rotor thrust is much greater and increases with wind speed in above-rated conditions, see Figure 4. However, by adjusting the pitching schedule with wind speed, the gradient in above-rated wind speed could be reduced and, thus, the fatigue loads on the support structure. This strategy would reduce C_p by an amount that varies with wind speed. However, that could be compensated for by increased utilisation of azimuthal variation in rotational speed. It should be noted that for floating turbines, a fixed pitch offset might not be advisable as the more important issue might be the general greater magnitude of the thrust.

By reducing the fixed pitch offset, see contours for $C_p=0.52$ and 0.51 in Figure 2, λ can be reduced for a relatively small reduction in C_p . Indeed, for $C_p=0.51$, a value of λ can be achieved that is not much different from that with no fixed pitch offset. The corresponding fixed-pitch offset is, also, reduced to approximately 5° . The reduction in C_p could again be compensated for by increased utilisation of azimuthal variation in rotational speed. It should be noted that, for floating turbines, the general greater magnitude of the thrust with a fixed pitch offset might be the more important issue, making this option less attractive.

The second option is not to use a fixed-pitch offset but rely solely on the azimuthal variation in rotational speed to increase energy capture. Indeed, the natural inclination might be to adopt this strategy, since it has little impact on the mechanical aspects of the turbine. Given that high wind speeds only occur with a much lower frequency than lower wind speeds, it could be preferable to hold the amplitude of the oscillation constant above some wind speed, say roughly 15m/s when the increase in power would be 10%.

As discussed in point 3 above, a rapid increase in pitch angle is required in wind speed just above rated, especially for the negative pitching strategy with a fixed pitch offset. Consequently, when switching from

below to above-rated operation, some anticipatory pitching, whilst still below rated, might be required. However, the inertia of the primary rotor is roughly 3 times that for an equivalent HAWT rotor. Consequently, the transient in rotor speed, arising from being slow to pitch in conditions just above rated, might significantly reduce or even eliminate the need for anticipatory pitching. The two negative pitching strategies both exhibit a pronounced peak in thrust at rated wind speed. Hence, anticipatory pitching might, also, be required to reduce these peaks.

Consider the primary rotor operating in some point below rated wind speed with the rotor speed corresponding to C_{pmax} tracking. An adjustment of pitch angle as discussed above would reduce the rotor torque. To maintain the balance between the primary rotor torque and the secondary rotor thrust, an accompanying adjustment is required to the constant λ curve tracked by the secondary rotors. Such an adjustment is always possible since it too corresponds to a reduction in aerodynamic efficiency in comparison to a situation with no adjustment to the pitch angle.

Although a fixed pitch offset might not be preferred in above rated wind speed, it could be attractive in below rated wind speed to increase the C_{pmax} . The offset would need to be unwound as rated wind speed is approached. In a similar manner to the anticipatory pitch adjustment, an accompanying adjustment is required to the constant λ curve tracked by the secondary rotors. Such an adjustment continues to be possible as the aerodynamic efficiency is again being reduced.

Determining which is the best strategy, requires a full assessment of the energy capture and loads. However, it also depends on the impact of the various options on the characteristics of the range of speed of PMSG generators and the control capabilities of their associated power electronics. For example, a PMSG running at above-rated rotor speeds will incur excessive magnetization of the windings leading in turn to higher generator terminal voltages. Any power electronic converter connected at the terminals of the generator will require an increased DC voltage bus to manipulate the voltages of the generator, as well as an extra power rating to handle the increased magnetizing currents. On the other hand, increased loading and magnetizing currents lead to higher resistive losses which increase the temperature of the generator. Based on the desired operation strategies presented in this section, a PMSG capable to work in cyclic over speed regimes up to 140-150% will be considered when developing internal characteristics of the generator.

3. Defining the rotor speed, ratings and dimension of the secondary Rotors

The design of the generators for the X-Rotor concept is driven primarily by the requirements of aerodynamics. The logic of the aerodynamic design of the secondary rotors, and how this influences the generator design is discussed briefly here.

Aerodynamic Factors

The X-Rotor concept (shown in Figure 5) differs significantly from typical wind turbine designs, most obviously in that the axis of rotation of the primary rotor is vertical rather than horizontal. The vertical axis rotor does not, however, directly drive any power take-off. Instead, secondary rotors, located on the lower arms of the primary rotor are used to generate electrical energy.

Despite energy being extracted by the secondary rotors, the overall efficiency of the rotor is strongly linked to the power coefficient of the primary rotor. Assuming that the rotor inertia is sufficiently high such that the change in angular speed over a single revolution is negligible, consider the revolution averaged torque on the primary rotor, given by,

$$\overline{Q}_P = \frac{P_P}{\omega} \quad 1$$



Figure 5: X-Rotor Basic Structure

Where P_p is the primary aerodynamic power and ω is the rotational speed of the primary rotor. For steady operating the efficiency of power conversion (η) becomes,

$$\eta = \frac{P_{Out}}{P_p} = \frac{N_r \bar{P}_s}{\omega N_r r_s \bar{T}_s} \quad 2$$

where N_r is the number of rotors, \bar{P}_s is the revolution averaged power of the secondary rotor, r_s is the radius of the secondary rotor, and \bar{T}_s is the rotor averaged thrust on the secondary rotor. It can be hence be derived that if the power increase obtained through the exploitation of azimuthal variations in flow speed is ignored,

$$= \frac{1 + \frac{3}{2} \lambda^{-2} C_{P_s}}{1 + \frac{1}{2} \lambda^{-2} C_{T_s}} \quad 3$$

Given that, for a reasonable value of λ , $1 + \frac{3}{2} \lambda^{-2} \approx 1 + \frac{1}{2} \lambda^{-2}$, the efficiency of power conversion can be approximated by,

$$\eta = \frac{C_{P_s}}{C_{T_s}} \quad 4$$

At this point, it is useful to reflect on the aerodynamic design of both the primary rotor and the secondary rotor. The primary rotor should be designed for optimal energy capture. The initial design detailed in [2] uses a primary rotor tip speed ratio of $4 < \lambda_p < 5.5$, with a rated wind speed of 12.66m/s. Hence, the tip speed of the primary rotor at rated wind speed, which is the mean wind speed experienced by the secondary rotor, will be approximately 60m/s.

60m/s is a much higher wind speed than that typically experienced by a conventional HAWT. As such, the design criteria for the secondary rotor differs significantly from that of a typical rotor. Further, due to the relationship of the efficiency conversion of the X-Rotor to the power and thrust of the secondary rotor, the design goal is not to maximise the power coefficient per se, but to maximise the ratio of power coefficient to thrust coefficient.

There is a further design criterion that must be considered, which is the speed of sound in air. It is known that aerodynamics at supersonic speeds differ significantly from lower speed aerodynamics and so the tip speed of the secondary rotor should not become too high. The noise of the rotors is also a consideration, with noise being directly linked to the speed of rotation. A sensible precaution is, therefore, to restrict the tip speed of the secondary rotors to around half the speed of sound.

Assuming basic actuator disc theory, the optimum thrust coefficient is given by,

$$C_{Ts} = 4a_s(1 - a_s) = \frac{A_p C_{pp}}{N_r \pi r_s^2 \lambda_p^3} \quad 5$$

where a_s is the induction factor, A_p is the primary rotor area, C_{pp} is the primary rotor power coefficient, N_r is the number of rotors, r_s is the secondary rotor radius and λ_p is the primary rotor tip speed ratio. The only variable that can be set by the secondary rotor design is the rotor radius r_s , which is constrained by the allowable tip speed, itself constrained by the speed of sound in air.

O&M, Parasitic Drag and Environmental Factors

Part of the economic case for the X-Rotor is the lower Operations and Maintenance (O&M) costs of the design. A key aspect of this is the direct drive approach, reducing drivetrain complexity. With the secondary rotors rotating much faster than traditional HAWTs, there are fewer poles required to facilitate a direct drive approach. By setting the generator frequency to 25Hz, a four pole-pair approach leads to a rotational speed of the secondary rotors that fits well with the aerodynamic demands.

Increasing the number of pole pairs (N_p) could allow a larger rotor radius for a given tip speed ratio by reducing the required rotational speed of the secondary rotor, as the secondary rotor speed ω_s is given by,

$$\omega_s = \frac{2\pi f_0}{N_p} \quad 6$$

where f_0 is the electrical frequency in Hz. Whilst this option is likely to be of benefit to the secondary rotor design when considered from an actuator disc standpoint, there are two main disadvantages with increasing the number of pole pairs.

Firstly, whilst the rotor size can be increased, the generator size also increases significantly, directly increasing the size of the hub required to house the generator. A larger hub will result in higher parasitic drag, moving the aerodynamics further from the ideal actuator disc assumption used in the previous analysis. Large hubs can also impact on the accuracy of Blade Element Momentum (BEM) code modelling of turbine rotors, with DNV Bladed warning that the empirical adjustment factors used to account for parasitic drag of the hub may not be valid if the hub diameter exceeds 10% of the rotor diameter.

Secondly, increasing the number of pole pairs increases the required rare-earth metals for construction of the X-Rotor. Rare-earth materials are expensive and the mining and refinement of such materials is often a source of significant pollution and CO₂ emissions. Additionally, the dominance in the rare earth market of China has led the EU and the USA to flag these materials as “being subject to potential supply risks and both are implementing strategies to mitigate such risks” [3]. The same reference states that “In the short term, the situation could be addressed through interventions aimed at reducing demand, such as alternative pathways for achieving policy targets, incentivising rare earth-free technologies and investing in research and innovation” [3]. Hence, it is desirable to limit the pole pairs to as low a number as possible.

Primary Rotor Led Design

There are numerous ways in which the previous configurations can be used to jointly inform the design of primary and secondary rotor design. However, as discussed previously, the overall efficiency of the X-Rotor is dependent upon the primary rotor design. Hence, a design method that considers the primary rotor first and uses this design to narrow the specification of the secondary rotor is a sensible approach.

Using the design of the primary rotor postulated in [2] narrows the design specification for the secondary rotor significantly.

Higher primary rotor tip-speed ratios for the primary rotor lead to lower secondary rotor tip-speed ratios. A turbine operating at a lower tip-speed ratio will typically be required to be a higher-solidity rotor which increases drag losses due to the larger blade area, higher solidity rotors will also increase losses associated with finite blade span effects. Finally, lower tip-speed ratio rotors will also increase the effect of tip-loss. For a typical X-Rotor type VAWT the operational tip-speed ratio may range between $4 < \lambda_p < 5.5$, and so, if the turbine is to be rated at a windspeed of 12.66m/s, the secondary rotor tip-speed ratio will range between $2.7 < \lambda_s < 3.7$.

Based on these assumptions, and on the use of four pole pairs for the generator, the rotor radius of the secondary rotor is likely to be between 4.4m and 5.6m. Ideally, the diameter of the generator should therefore be less than one metre and, if this cannot be achieved, the diameter should be as small as possible.

4. Initial assessment of PMSG requirements.

Type-IV direct-drive wind generators using permanent magnet synchronous generators and fully rated power electronic converters have become an attractive choice for megawatt-level wind turbine systems. Although generators and power electronic systems can be designed to operate in a wide variety of voltages and current ratings, standardized design practices allow some degree of compatibility between brands. Such standards include rated generator voltage level, rated DC bus voltage for power electronics, type of power electronic topology and maximum current levels. The design of the secondary rotors uses as a starting point the design standards and commercial type-IV wind generators, seeking to maximize their compatibility with commercially available components.

The first design standard to consider is the rated voltage at the PMSG generator terminals, if this value is chosen correctly, then the generator will be capable to interconnect with commercial power electronic converters. The standard rated voltage of the generator is mainly defined by the power rating of the machine and cost considerations. Table I shows a listed commercial PMSG wind turbine generators, their voltage rating, power level and associated power electronic architecture.

Table I List of Standard Ratings of Commercial PMSG Wind Turbines [4]

Manufacturer	Model	Power	Rated Voltage	Power Electronic Topology
Enercon	E126	7.5 MW	690V	Topology 1
Gamesa	G128	4.5 MW	690V	Topology 1
Winwind	WWD3	3.0 MW	690V	Topology 1
GE	2.5XL	2.5 MW	690V	Topology 1
Avantis	AV928	2.5 MW	690V	Topology 1
Areva	M5000	5.0 MW	3300V	Topology 2
Converteam	MV7000	7.0 MW	3300V	Topology 2
ABB	PCS6000	6.0 MW	3300V	Topology 2
Clipper	Britannia	10 MW	3600V	Unknown
Sway AS	ST10	10 MW	3500V	Unknown
Siemens	SWT7.0	7 MW	3300V	Unknown
Nordex	N150	6 MW	3300V	Unknown
XEMC-Darwind	XE/DD115	5 MW	3300V	Unknown
Marvento	M3.6	3.6 MW	3900V	Unknown
Clipper	C89	2.5 MW	690V	Topology 3
Vensys	V70/77	1.5 MW	690V	Topology 3

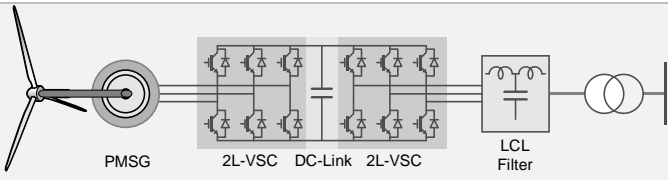
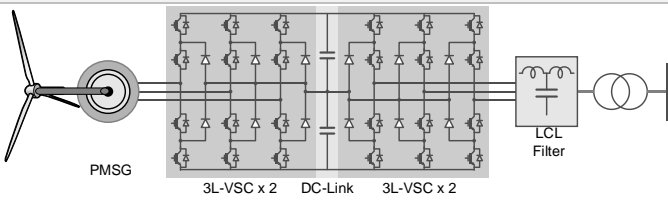
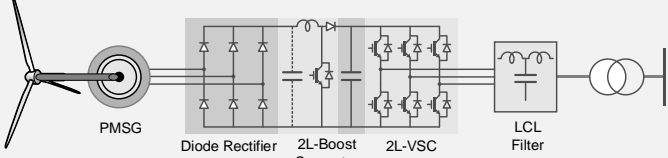
Goldwind	GW70/77	1.5 MW	690V	Topology 3
----------	---------	--------	------	------------

As seen in Table I, most of the commercial PMSG operate either at 690V or 3.3KV, which is consistent with the standard voltages defined for AC and DC electricity supply systems defined by the IEC (see Table II). The table also indicates that the commercial choice of voltage level is somehow linked with the power rating of the generator, where larger power-rating generators prefer to use larger rated voltage levels. Notwithstanding, the table indicates that some manufacturers prefer to stick to lower terminal voltages even for higher power ratings. This has to do with the manufacturers' choice of power electronic topology for their turbines, among other things. The definitions and circuit diagram of the topologies listed in Table I are presented in Table III.

Table II Regional Classification of low and medium voltages [5, 6]

Region	Standard	Voltage Class
Europe	IEC60038	Low Voltage Class (<1000V) 200V, 400V, 690V
		Medium Voltage Class (1KV-35KV) 3.3KV, 6.6KV, 11KV, 22KV, 33KV
North America	ANSI C84.1	Low Voltage Class (<600V) 208V, 120/240V, 480V, 575V
		Medium Voltage Class (600V-35KV) 2.4KV, 4.16KV, 6.9KV 12.47KV, 13.81KV, 21KV, 34.5KV

Table III Power Electronic converter topologies

Power Electronics Topology Type	Diagram
Topology 1 2-Level Back to Back Voltage Source Converter	
Topology 2 3-Level Back to Back Neutral point Clamped Voltage Source Converter	
Topology 3 Passive Front-end Converter	

Topology 1 is very popular for power electronic systems and has been successfully applied by manufacturers for many years. It has proven effective and cost-efficient for many applications, including wind generators. This topology is, however, less efficient and less reliable at AC voltage levels beyond 1KV. This is because the power electronic switches are subjected to the full voltage level of the DC bus, which needs to be larger than twice the peak AC voltage, and if this DC voltage level is excessively high the switches suffer extra stress when commuting as well as extra switching losses. Because of this limitation, several manufacturers prefer to use low voltage generators even for higher power ratings.

This requires the parallel connection of several 2-level back to back converters to handle the large current outputs of high power machines. Although this approach adds extra complexity in control to deal with circulating currents among converters, it provides a good level of redundancy in the drivetrain.

Topology 2 is capable of interfacing larger AC voltages because its internal configuration subjects the switches of the converter to only half of the DC voltage level. This topology, however, requires more power electronic devices and a more complicated control system. Topology 2 is a mature technology used extensively in the electric drive industry, however, several turbine manufacturers have been reluctant to move to higher generator voltage levels due to the reduced industrial experience. A cost analysis presented in [7] suggests that the cost of energy production can be decreased by 4 to 25% with MV operation.

In the PMSG the rotor flux is generated by permanent magnets and rotor field excitation, respectively. For this reason, the generator-side power conversion system in the PMSG/WMSG wind turbines can be realised using passive converters such as Topology 3. This topology has been introduced as a cost-effective solution to interface variable speed generators to the AC grid. The diode-bridge rectifier found in this topology is less expensive and inherently more reliable compared to the 2 or 3-level VSCs. The use of a passive generator-side converter is associated with some disadvantages. The generator currents contain significant 5th (14%) and 7th (7%) harmonics and this leads to 6th harmonic distortion in the electromagnetic torque [8, 9]. Topology 3 has found some commercial success in Enercon (e-82E3), Vensys (V70/77) and Goldwind (GW70/77) wind turbines however its applications is still limited in the wind power industry. For the specific case of the X-rotor, the reduced inertia of the secondary rotors may increase the effect of the torque ripple in the vibration and speed of the machine. Because of this, topology 3 is not being considered as candidate for the secondary rotor drivetrain.

A summary of the characteristics of topologies 1 and 2 for low and medium voltage, adjusted for a PMSG power rating of 2.5 MW, are presented in Table IV.

Table IV Summary of power electronic converter characteristics for LV and MV 2.5 MW generators

Feature	Low voltage Generators	Medium Voltage Generators
Typical topology	Topology 1	Topology 2
DC voltage	Around 1200V	Around 5300 KV
Parallel topologies	4	None
Rated DC current	2510 A	480 A
Circulating currents between parallel topologies	High	None
Power Quality	Medium	Low
Maintenance cost	Low	Low
Redundancy	High	Low
Cost (data from 2012 for 3MW converter [10])	\$149,222.81	\$118,386.66
Market status	Mature	Available/Emerging

With regard of the efficiency of the different power electronic topologies Figure 6 shows the efficiencies of the rectifying (i.e. the machine side converter) and inverting (i.e. the grid side converter) for both topologies. As seen in Figure 6 a) the whole system efficiency of topology 1 is dominated by the rectifier losses on light loads. In topology 2 the efficiency at full load is better than in topology 1 as seen in Figure 6 b). This means better efficiency for topology 2 at rated power also smaller heat sink and better reliability.

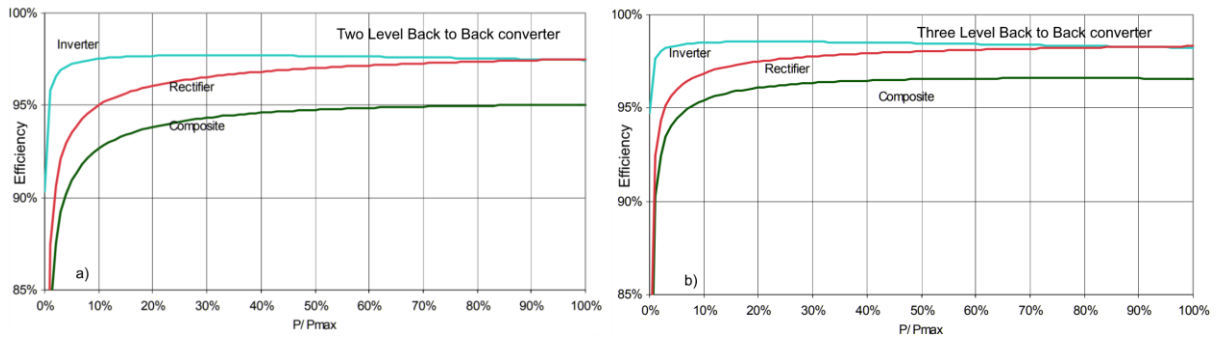


Figure 6 Efficiency of power electronic converters a) Topology 1. b) Topology 2. [11]

Besides the power electronic converter topology, there are other factors that define the choice of the generator voltage, this includes generator and cable cost as well as transformer size. A summary of such design choices is presented in Table V adjusted for a PMSG power rating of 2.5 MW

Table V Summary of design choices for Low Voltage and Medium Voltage operation for a 2.5MW wind generator

Feature	Low voltage Generators	Medium Voltage Generators
Typical Voltage	690 V	3.3KV
Cost of generator	Medium	Medium-High
Cable size and cost	High	Low
Transformer size	Medium	Low
Grid filter size	Medium	Low
Recommended power Rating according to academic literature [8]	0.5-3 MW	3-6 MW

Concluding remarks

Academic literature favours the use of Low voltage generators for power levels up to 3MW, however the review of current industrial practices evidences that there are well-grounded reasons to transition to a medium voltage devices. Because of this, this work package will use both approaches (LV and MV) to generate optimal generators constructions. The final choice of generator voltage level will depend on the results of the optimization, in terms of conformity with cost, size and efficiency. Another factor that will influence the final choice of voltage level for the generator is the capability of the power electronic topology to handle the overvoltage and overcurrent's produced by above rated operation.

5. PMSG generator design using heuristic methods

PMSG design strategies and considerations

An optimal design of PMSG involves the right selection of at least 12 variables related to the construction and magnetization of the generator. Such variables are, in turn, shaped by the initial specifications of the machine, type of material used, the technological constraints of the manufacturing process and by user-defined restrictions. Optimality is obtained when the selection of variables meets an objective function, which could be related the material cost, dimension, efficiency, temperature performance, or a combination of those. The search for optimality is usually carried out using metaheuristic algorithms that iterate a long list of design procedure equations. Examples of design methodologies are presented in detail in [12-15].

The design variables to optimize for a PMSG are listed in Table VI along with a description of the effects of the variable in the design of the generator.

Table VI Design variables in the design of PMSG

Variable	Units	Effects on parameters of generators [14]
Linear electric loading, J_l	A/m	Specific electric loading, J_l represents the total effective value of ampere turns in stator slots per stator periphery length. J_l relates to thermal loading and torque density. Large values of J_l lead to large torque density, and consequently to smaller machine size, which may end up in machine overheating and lower efficiency.
Airgap flux density, B_{ag}	Teslas	Permanent magnet (PM) airgap flux density, varies from 0.2 T in micromotors to 1 T in large torque density designs. Together B_{ag} and J_l determine the volume of the machine for given base torque.
Stator teeth flux density, B_{st}	Teslas	Stator tooth flux density determines the degree of magnetic saturation in the machine it varies from 1.2 to 1.8 T, in general, for silicon laminated stator cores.
Stator yoke flux density, B_{sy}	Teslas	Stator yoke flux density is chosen as a compromise between the level of magnetic saturation and the limitations due to core losses. Small values of B_{sy} may lead to a larger machine size and weight, especially if the number of poles is small
Rotor yoke flux density, B_{ry}	Teslas	Rotor yoke flux density is important in the machine with a large number of poles (and a large diameter) when the PMs are not any more placed directly on the shaft.
Stator current density, J_s	A/mm ²	Current density, determines the copper losses and the copper volume. Thin and deep slots that have small values of J_s (2–3.5 A/mm ²) may lead to a high leakage inductance and machine volume (and weight). On the other hand, high J_s values (>8 A/mm ²), in general, not only imply forced cooling but also lead to lower efficiency while reducing the machine volume.
Machine shape factor, or core stack length per pole pitch $\lambda_c = l_{stack}/\tau$	Units	Machine shape factor, is the ratio between the axial (stack) length of the machine l_{stack} and the pole pitch, λ_c . This variable affects the diameter and length of the generator.
Slots per pole per phase, q_1	Units	Number of slots per pole per phase.
Slot opening, s_o	mm	The minimum value of slot openings is limited by the possibility to introduce the coils, turn by turn, in the slot and by the increase of slot leakage inductance and PM flux fringing. Its maximum value is limited by the PM flux reduction, cogging torque increase, and torque ripple.
Tooth top height, H_{s4}	mm	The minimum value of H_{s4} is limited by technological (and magnetic saturation) constraints and its maximum value is limited by the increase the slot leakage inductance.
Coil span per pole pitch, y_1	Per unit	Coil span is the distance between the forward and return sides of the coil; it may be measured in mm but also in number of slot pitches
Embrace or Ratio of PM width to pole pitch α_m	Per unit	Affects the permanent magnet flux per pole value. Failing to realize the required PM flux per pole implies larger currents for the based torque, leading to higher losses and extra copper weight.

The initial specification of the machine are the starting point for the design of the PMSG, such specifications are listed in Table VII

Table VII Initial specifications for PMSG design

Parameter	Unit	Variable
Base continuous power	Watt	P_b
Base Frequency	Hz	n_b
Nominal phase voltage	Volts	V_n
Nominal speed	RPM	n_{max}
Power at Nominal speed	Watts	P_{max}
Number of phases	Units	m
Number of pole pairs	Units	pp
Number of Parallel current paths	Units	$Parallel_p$
Desired power Factor	Units	Ip_f

The technological constraints are related with the capacities of manufacturing machines and constraints generated by materials when manufacturing the different elements of the generators. Table VIII list the minimum and maximum values of the technological constraints as well as other constants used for the design of the PMSG and the reasons behind the given limits.

Table VIII technological constraints and constants applied to the optimization algorithm

Variable	Minimum Value	Maximum Value	Units	Reasons for limits [12, 14].
Optimization variables				
Linear electric loading, J_l	15	30 <60	kA/m	Specific magnetic and electric loadings are limited by the properties of the materials (iron for the flux, and copper for the current), and by the cooling system employed to remove heat losses.
Airgap flux density, B_{ag}	0.45 0.61	0.75 1.05	Tesla	Limits set by the saturation in the lamination.
Stator teeth flux density, B_{st}	1	2 <2	Tesla	Limits set by the laminated stator cores
Stator yoke flux density, B_{sy}	0.9	1.9 <2	Tesla	Avoids designing unusually big machines
Rotor yoke flux density, B_{ry}	0.9	2.1 <2	Tesla	Avoids designing unusually big machines
Stator current density, J_s	3	8 6	A/m m ²	Upper limit set by to avoid forced cooling in generators.
Machine shape factor, λ_c	0.5	3	Per unit	larger stator outer diameter and pole number are preferable against larger stack length
Slots per pole per phase, q_1	2	4	units	Limits set avoid large synchronous parasitic torques and radial forces

Slot opening, s_o	1 4	5 4	mm	The minimum value of s_o is limited by the possibility to introduce the coils, turn by turn, in the slot and by the increase of slot leakage inductance and PM flux fringing. Its maximum value is limited by the PM flux reduction, cogging torque increase, and torque ripple.
Tooth top height, H_{s4}	0.5	2	mm	The minimum value of H_{s4} is limited by technological (and magnetic saturation) constraints and its maximum value is limited by the increase the slot leakage inductance.
Coil span per pole pitch, y_1	0.66 0.8	1 0.8	Per Unit	1 Per unit indicates full pitch windings.
Embrace or Ratio of PM width to pole pitch α_m	0.5	1	Per Unit	The magnet angle is allowed to be in the range between 0.5 (50% percent of the pole is covered with permanent magnets) and 1 (the entire pole is covered with permanent magnets).
Other technological design variables				
Iron fill factor (staking factor) sf	0.97 0.9	0.97	Per unit	Limit set by lamination width
Slot fill factor $sSlotFill$	0.33 0.65	0.7 0.65	Per unit	lower values correspond to using semiclosed slots with coils introduced, turn by turn, in the slot, while larger values correspond to open slots and premade coils made of conductors having rectangular cross sections.
Wedge angle s_α	22.5	22.5	Deg	Limit PM flux density fluctuations
Slot insulation thickness $sInlTh$	0.15	0.15	mm	Data defined by manufacturing process
Thickness of slot closure (wedge) $sInlClosTh$	0.5	0.5	mm	Data defined by manufacturing process
Right part of overhang coils lfl	8 (suggested)	8 (suggested)	mm	User defined value
PM overlength $dlpm$	2 (suggested)	2 (suggested)	mm	User defined value to calculate more accurately the rotor core length
Flux density saturation factor k_s	1 (suggested)	1 (suggested)	Per unit	flux density is directly proportional to the saturation factor
Generator overload factor kl	-	-	Per unit	User-defined value. Used to define The PM thickness to produce a certain PM flux density in the airgap and also to avoid demagnetization under a given overload
Winding layers	1	2	Units	In single winding layers the complete slot contains only one coil side of a coil. Here

wls				insulation can be properly applied which is advantageous for high voltage machines. Double layer winding can lead to more savings in copper material and lower leakage reactance
------------	--	--	--	--

The initial specifications and design variables are used as inputs for the PMSG design methodology and optimization procedures. This research has selected the design methodology presented in section 9.6 of [14] given its recency and the authoritative nature of the designer* and will not be reproduced here again. Figure 7 PMSG design methodology proposed in [14] shows a flow diagram of the design methodology used in this research.

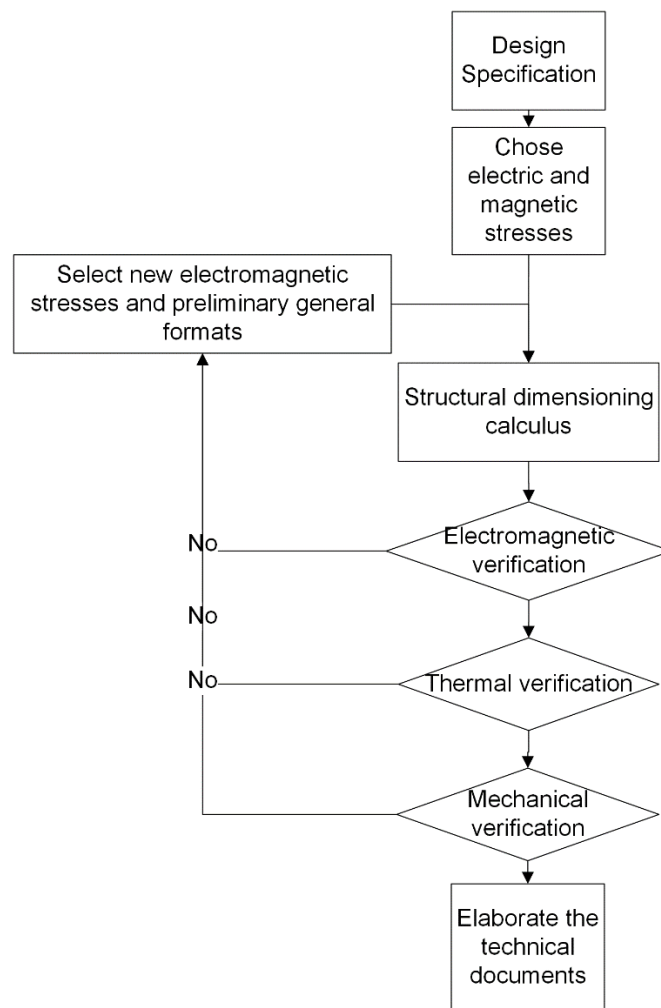


Figure 7 PMSG design methodology proposed in [14]

The cost function for the design optimization has been selected in the light of the requirements of efficiency and size for the generators of the X-rotor, the cost function is also shaped by the usual requirements in reducing initial costs (i.e. cost of active materials) and as it is usual in wind generators, cost of motor weight. The cost function also adds penalty for overtemperature to avoid the design of highly temperature sensitive generators. The initial costs are calculated as follows

* Professor Ion Boldea, IEEE Fellow and Recipient of the IEEE 2015 Nikola Tesla Award for Contributions to the design and control of rotating and linear electric machines for industry applications

$$C_i = m_{cu}p_w + m_{Fe_a}p_{lam} + m_{PM}p_{PM} + C_{pass} \quad 7$$

where m_{cu} , m_{Fe_a} , m_{PM} and m_{Fe_p} are the weights in kg of the copper windings, the active material weight (including the rotor yoke weight, the stator yoke weight, the stator teeth weight and the stator core weight), and the permanent magnet weight. p_w , p_{lam} and p_{PM} are the copper, lamination and PM unitary prices in EU/kg. C_{pass} is the cost of passive materials (e.g. bearings, shafts, frames, ventilation systems, winding terminals and terminal boxes) and is calculated as a cost proportion of the total weight of the machine (i.e. $C_{pass} = \text{price of passive materials} * \text{total weight of generator}$).

The cost of losses is calculated as

$$C_E = p_e n_y h_{hy} \left(\alpha_r \left(\frac{1}{e_r} - 1 \right) P_N + \alpha_{or} \left(\frac{1}{e_{tan}} - 1 \right) P_{or} \right) \quad 8$$

where p_e is the energy cost in EU/kWh, n_y is the number of operational years of use the generators, which should be consistent with the desired lifespan of the X-rotor system, h_{hy} is the annual operational hours of the generators which is set by the usual capacity factor of offshore wind turbines (see [16] for estimation), α_r is the probability of the generator to operate rated power loads and can be decreased in case the generator is mostly working at below rated conditions, e_r is the calculated efficiency of the machine at rated power, P_N is the rated power of the generator. α_{or} is the probability of the generator to operate at over rated power loads and can be different from zero in case the generator has some degree of cyclic overloading, a probabilistic analysis of the X-rotor operation can be used to define the value of α_{or} , e_{ro} is the calculated efficiency of the machine at a given overrated power level, P_{or} is the given over rated power of the generator.

Low weight is an important factor for wind generators, as such, it may be important to avoid low-cost but large machine weight solutions. In order to force the algorithm to reduce the generator weight a cost could be added to the cost function as

$$C_m = m_t p_m \quad 9$$

where $m_t = m_{cu} + m_{Fe_u} + m_{PM}$ is the motor weight and p_m is the associated structural cost of supporting larger generators. Future work in the structural design of the X-rotor will define if C_m should be added to the optimization machine design.

The cost function also includes a penalty cost for overtemperature to avoid generator design solutions prone to overheating. This penalty cost is set to vary linearly with the overtemperature and is defined as

$$C_E = \begin{cases} k_T (T - T_{max}) C_i & \text{if } T > T_{max} \\ 0 & \text{if } T \leq T_{max} \end{cases} \quad 10$$

where k_T is a overtemperature penalty cost coefficient in per unit, C_i is the initial cost defined in (7), T_{max} is the maximum winding temperature in centigrade and T is the calculated temperature of the machine a full power, defined as

$$T = \frac{P_{cu} P_{FE}}{\alpha_r A_{frame}} + T_{amb} \quad 11$$

where P_{cu} is the resistive losses of the windings in watts, P_{FE} the sum of the Iron core losses and the Iron teeth losses, α_r is the thermal transmission coefficient in W/m²*deg, T_{amb} is the ambient temperature or the temperature of the cooling liquid and A_{frame} is the Thermal equivalent frame area (m²) of the generator defined as:

$$A_{frame} = \pi \cdot sDo \cdot l_{frame} \cdot k_{ff} + \frac{\pi}{2} sDo^2 \quad 12$$

Where sDo is the stator outer diameter in meters, l_{frame} is the effective length of the generator frame in meters, k_{ff} is the increasing factor of cooling surface in per unit.

Additionally an artificial cost restriction is added to the cost function to de-incentivize solutions with larger stator diameters. Setting a desirable stator diameter to 2000mm C_E is modified in the following way

$$C_E = \begin{cases} C_E & \text{if Stator outer diameter} < 2000 \text{ mm} \\ 1.5C_E & \text{if Stator outer diameter} > 2000 \text{ mm} \end{cases} \quad 13$$

Using equations 7,8,9 and 13 the total cost is calculated as:

$$T_{cost} = C_i + C_E + C_m + C_{temp} \quad 14$$

Equation 14 can be treated as a complex objective function for a metaheuristic optimization problem. In this research, genetic algorithms are used to obtain optimized results using Equation 14 as a fitness function. The details of the genetic algorithms and their application for the design of the secondary generators are presented next.

PMSG design exercise using genetic algorithms

A Genetic Algorithm (GA) starts with particles distributed randomly within the solution space and assesses each against the 'fitness function' (aka. the objective function). The best set of solutions, say top 20%, are selected in a survival-of-the-fittest manner to be the 'parents' of the next generation of solutions. There are many ways these solutions can be carried forwards. Typically the parents are cloned (or kept) for the second iteration. The 'offspring' solutions are made from two parent solutions and can be 'mutated' (or slightly altered) to introduce some stochasticity into the iteration - these may make up 60% of the next iteration solutions. The final 20% of solutions in this example is from newly generated random solutions. The algorithm tends towards the 'fittest' or best solution through this evolutionary approach [17].

The genetic algorithms consider a population np of candidate solutions evolution under specific selection rules to a state that minimizes the cost function a random number, p_{rand} , between zero and unity is generated. The index, k , of the smaller rank, rk , larger than the random number, p_{rand} , is chosen to be the first parent. For the second parents, another random number is generated and it is chosen using the same method. In this way, more adapted members have a chance to become parents and transmit the genetic information to the next generation. The first populations are very nonhomogeneous populations, and, using only this method to transmit genetic code through to the next generation, produces a rapid convergence where the generality is lost. In order to avoid a rapid convergence to a local solution, the fitness function of the members that are already parents is multiplied by an exclusion factor ke . In this way, the chance to become parents again is reduced. Two offsprings are produced by crossovers before they go to the next generation, this is done by recombining the genetic code of from two parents. Randomly, a part of the offspring suffers genetic mutation before it goes to the next generation, this is controlled by the mutation factor rm . The members of the old generation are ranked again and then the process to produce new members is continued until a new, complete, generation is produced. The new generation will take the place of the old generation and the algorithm is repeated until the given number of generations ng is reached.

Figure 8 shows the flow diagram of the genetic algorithm-based procedure used to search for optimal design parameters for the PMSG or the X-rotor.

Using the restrictions defined in Table VII and the design methodology presented in [14], two particle swarm optimization processes were generated using the initial inputs and data.

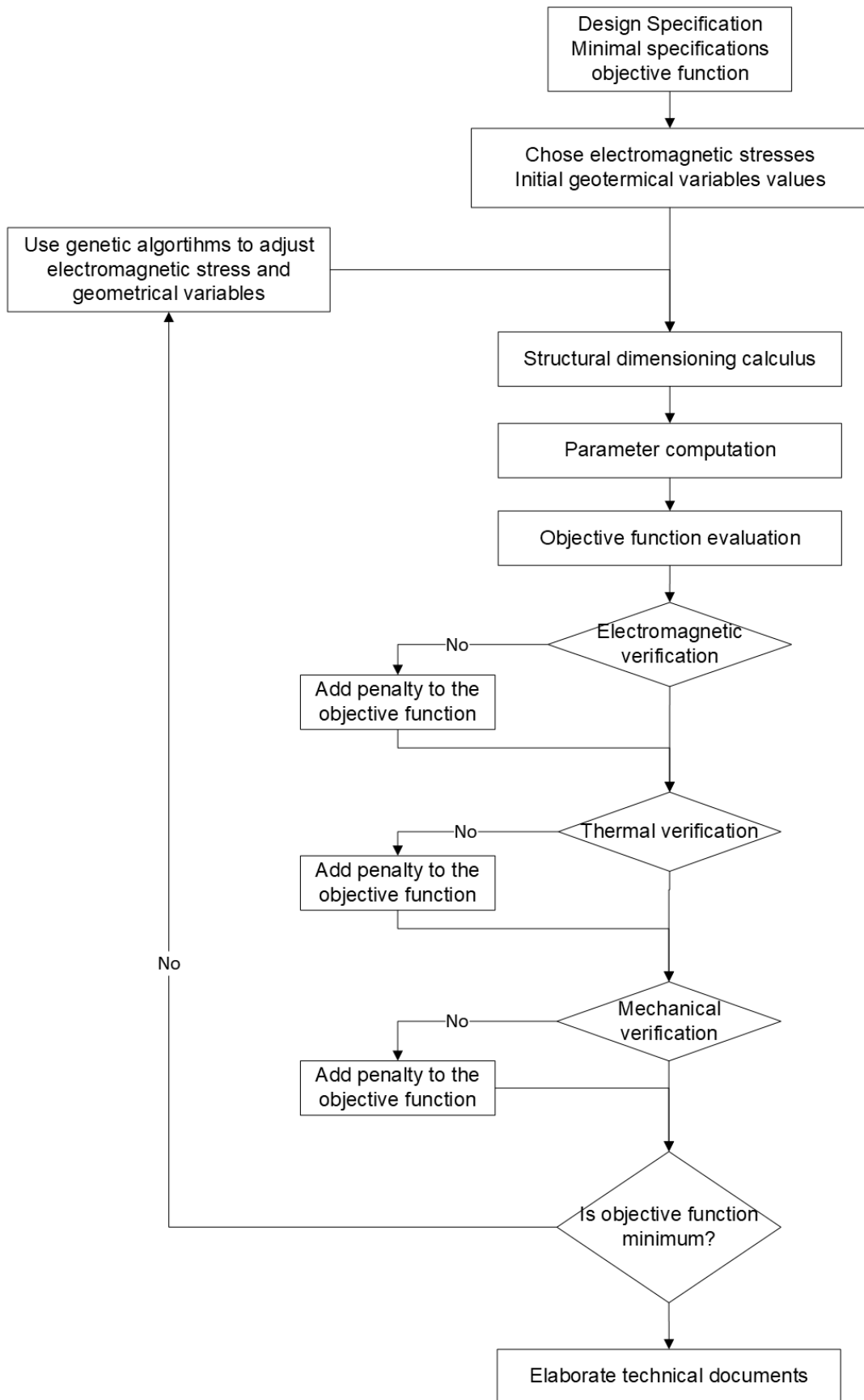


Figure 8 Genetic algorithm-based procedure used to search for optimal design parameters for the PMSG

Table IX Initial parameters provided as inputs to the optimization algorithm

Parameter	Unit	Variable	Exercise 1	Exercise 2
Base continuous power	Watt	P_b	2.5e6	2.5e6
Frequency	Hz	n_b	25	25
Maximum phase voltage	Volts	V_n	690	3300
Overload factor	Per Unit	k_1	0.9	0.9
Nominal speed	RPM	n_{max}	375	375
Power at nominal speed	Watts	P_{max}	2.5e6	2.5e6
Number of phases	Units	m	3	3
Number of pole pairs	Units	pp	4	4
Number of Parallel current paths	Units	<i>Parallelp</i>	1	1
Desired power Factor	Units	Ipf	0.95	0.95

For Both exercises the technological constrains and constants in Table X where used

Table X Technical Constraints and constants provided as inputs to the optimization algorithm

Optimization Variables	Min Value	Max Value	Minimum Variation
Linear electric loading, J_l	15	30	0.2
Airgap flux density, B_{ag}	0.45	0.75	0.01
Stator teeth flux density, B_{st}	1	2	0.05
Stator yoke flux density, B_{sy}	0.9	1.9	0.02
Rotor yoke flux density, B_{ry}	0.9	2.1	0.02
Stator current density, J_s	3	8	0.1
Machine shape factor, λc	0.5	3	0.1
Slots per pole per phase, q_1	2	4	1
Slot opening, s_o	1	5	0.2
Tooth top height, H_{s4}	0.5	2	0.1
Coil span per pole pitch, y_1	0.66	1	0.05
Embrace or Ratio of PM width to pole pitch α_m	0.5	1	0.01
Other design variables		Value	
Iron fill factor (stating factor) sf		0.97	
Slot fill factor $sSlotFill$		0.7	
Wedge angle s_α		22.5	
Slot insulation thickness $sltInlTh$		0.15	
Thickness of slot closure (wedge) $sltClosTh$		0.5	
Right part of overhang coils lfl		8	
PM overlength $dipm$		2	
Flux density saturation factor k_s		1	
Generator overload factor kl		1.8	
Winding layers wls		1	

Additionally, for both exercises the thermal specification (for thermal losses calculation) in Table XI were used.

Table XI Thermal specifications for the optimization problem

Thermal specification	Units	Values
Nominal stator winding temperature T_{wl}	Centigrade	105
Rotor PM temperature T_{pm}	Centigrade	100
Maximum Winding Temperature T_{max}	Centigrade	155
Ambient Temperature or cooling fluid temperature T_{amb}	Centigrade	50
Thermal Transmission coefficient α_r	W/(m ² *deg)	14.2

		(usual values are 14 for unventilated frames to 100 for water cooled frames)
Increasing factor of cooling surface k_{ff} (by use of fins to increase the surface area)	Units	3
Iron losses factor (factor larger than 1 due to field non-uniformities) k_{pf}	Per Unit	1.45
Assumed Mechanical losses P_{mech}	W	12500 Estimated as 0.5% of P_b

The genetic algorithm objective function follows equation 14, the value of the coefficients used for this function are listed in Table XII.

Table XII objective function coefficients

Coefficient	Value
EUR/kg copper price p_w	10
EUR/kg lamination price p_{lam}	5
EUR/kg PM price p_{PM}	50
EUR/kg energy price p_e	0.1
EUR/Kg price of passive materials p_{pass}	5
EUR/kg structural cost of supporting larger generators p_m	0 [†]
Hours per year of use h_{hy}	4000 [16]
Years of use n_y	25
Over temperature penalty cost coefficient k_T	1

Finally, the materials used for the lamination and PM where silicon electrical steel and Vacodym 677 NdFeB Magnets [18].

Optimization Results for the 3.3KV generator

The evolution of the genetic algorithm is shown in Figure 9.

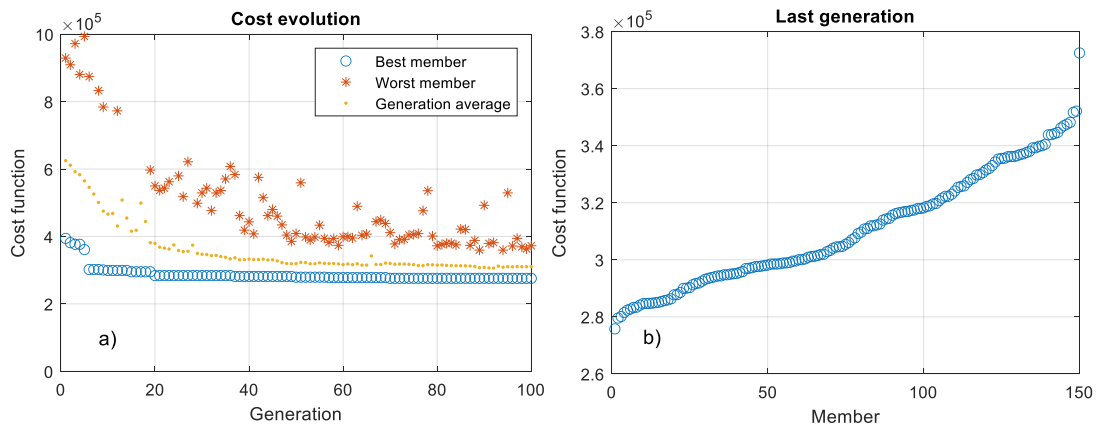


Figure 9 Evolution of the genetic algorithm for the 3.3KV generator design. a) selected members from each generation. b) All the members of the last generation.

As seen in Figure 9 a) every generation has a member (from the total number of members in the generation) that is best fitted for the required optimum criterion (blue circle), which minimizes the cost

[†]This value is not accounted for in the optimization exercise but can be revised after a detailed analysis of the structure of the X-rotor and the cost implications of supporting heavier generators.

function. All the members of the generation are characterized by the average cost function (yellow dot). For each generation, there is also a least-adapted member (red asterisk). Converge is appreciated as the generation number increases. Figure 9 b) Shows the performance of the all members of the last generation of the genetic algorithm process where member 0 is the best fitted for the required optimum criterion and member 150 is the least adapted member.

The evolution of the core design variables for the design of the 3.3KV PMSG is shown in Figure 10.

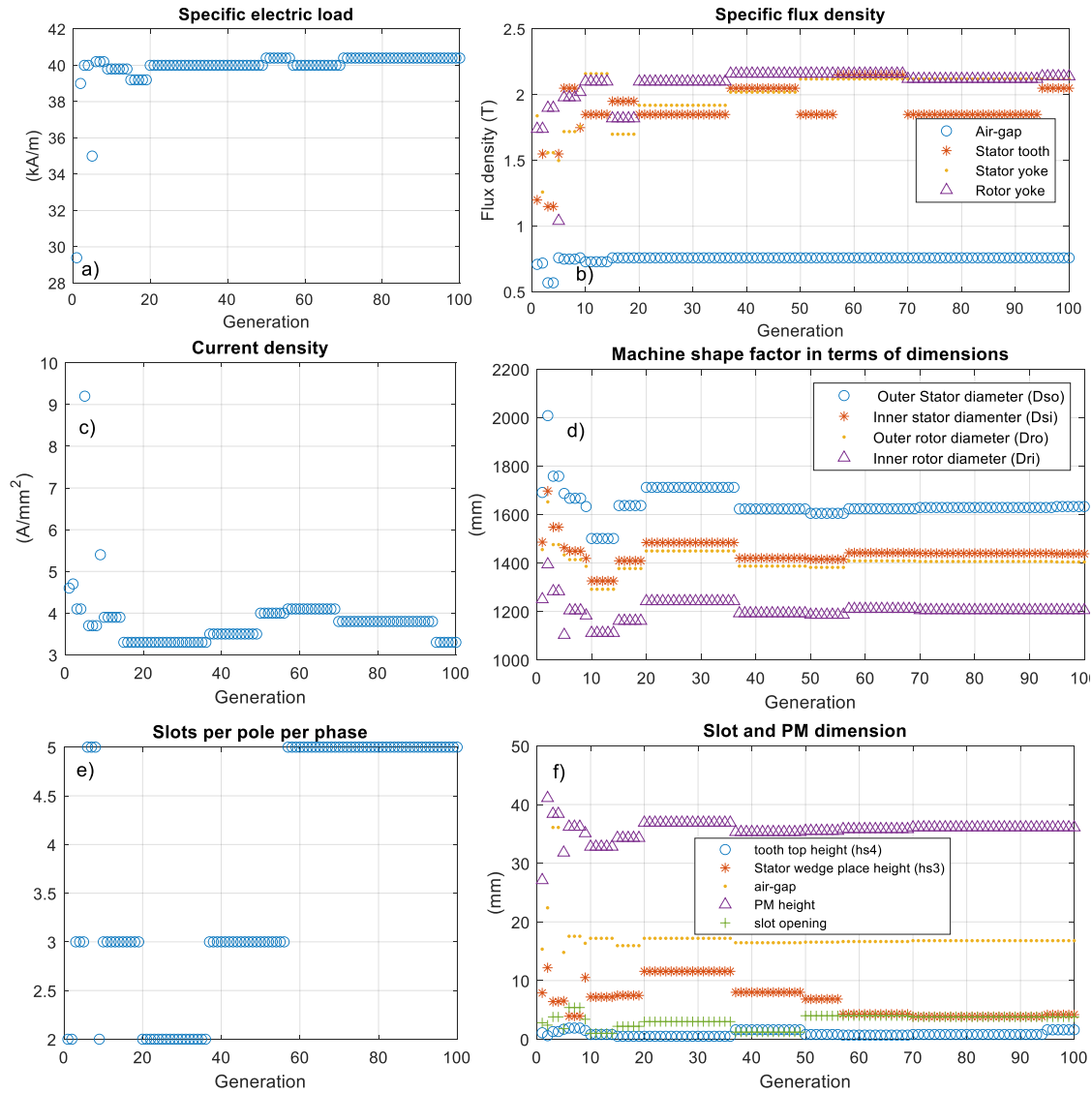


Figure 10 Evolution of design variables for the 3.3KV generator a) Electric load b) Flux densities c) Current density d) Dimensions e) slots per pole per phase f) slot dimension

Figure 11 shows the evolution of the performance and cost-related variables of the PMSG design.

Table XIII list the values of the best member of the final generation of the genetic algorithm. This values are treated as the optimized and used for the design of the 3.3KV PMSG.

Table XIII Results of the genetic algorithm optimization for the 3.3KV PMSG

Optimized Variable	Units	Optimized value
Linear electric loading, J_l	A/m	40.40e3
Airgap flux density, B_{ag}	Teslas	0.76

Stator teeth flux density, B_{st}	Teslas	2.05
Stator yoke flux density, B_{sy}	Teslas	2.12
Rotor yoke flux density, B_{ry}	Teslas	2.14
Stator current density, J_s	A/mm ²	3.3
Machine shape factor, or core stack length per pole pitch $\lambda_c = l_{stack}/\tau$	Units	2.2
Slots per pole per phase, q_1	Units	5
Slot opening, s_o	mm	3.8
Tooth top height, H_{s4}	mm	1.6
Coil span per pole pitch, y_1	Per unit	1
Embrace or Ratio of PM width to pole pitch α_m	Per unit	0.5

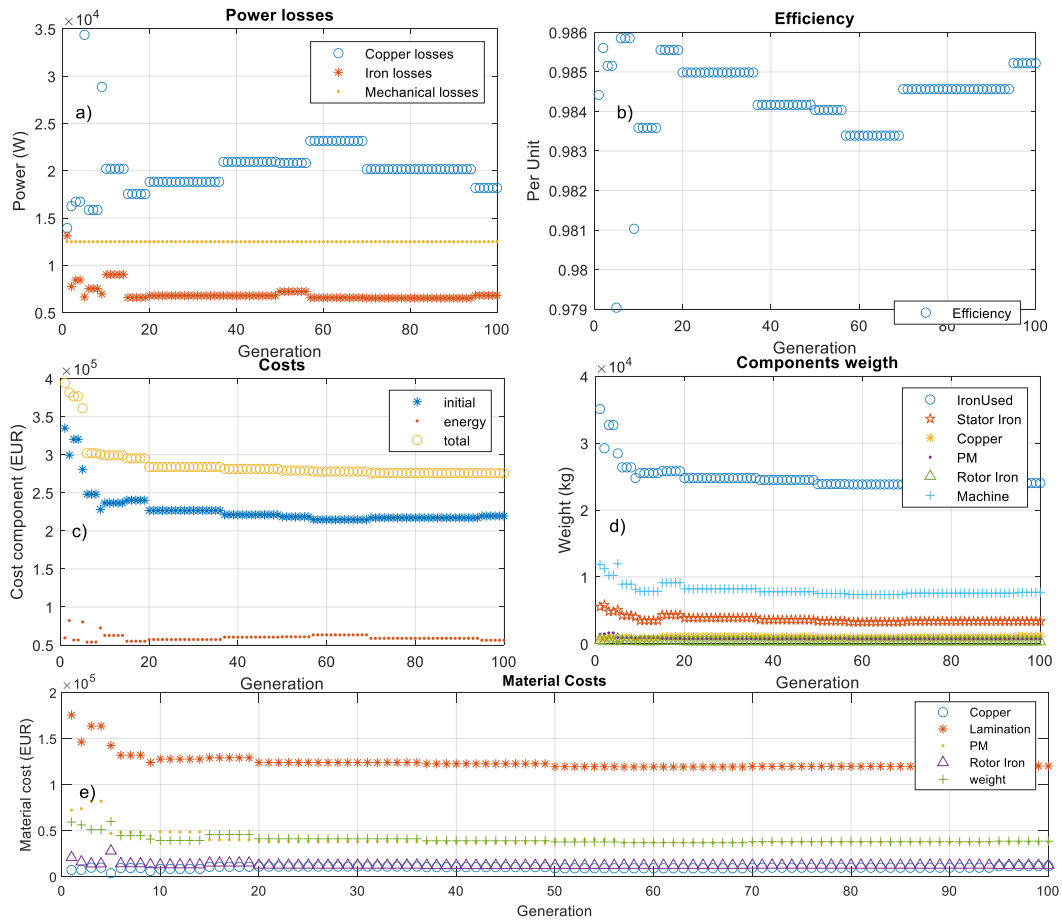


Figure 11 Performance and cost related variable evolution for a 3.3KV generator a) power losses b)Efficiency c) Costs d) Weights e) Material costs

Table XIV list the results of using the optimized variables in the design process of the PMSG, including the calculated efficiency, size, weight and cost.

Table XIV PMSG design parameters of the 2.5MW 3.3KV using optimized variables

Design Parameter	Optimized Value	Units
Rated power	2.5e6	Watts
Rated Frequency	25	Hz
Rated Phase Voltage	1905.25 (3.3KV/sqrt(3))	V
Iq rms current	526.06	A
Rated copper loss	18183.207	W
Rated Iron loss	6823.89	W

Rated Mechanical Loss	12500	W
<i>Rated Efficiency</i>	<i>0.9852</i>	<i>Per Unit</i>
Constructive Dimensions		
<i>Stator outer diameter</i>	<i>1633</i>	<i>mm</i>
Stator inner diameter	1438	mm
Stator tooth pole tip height	1.6	mm
Stator wedge place height	4.1828	mm
Overall slot height	33.059	mm
Stator yoke width	64.44	mm
Stator tooth width	13.95	mm
Air-gap height	16.8	mm
PM height	36.1	mm
Machine shape factor	2.2	Units
Stator coil height	26.62	mm
Stator slot width (root)	25.42	mm
Stator coil width (top)	24.03	mm
Stator slot mouth	3.8	mm
Radius of tooth head	724.78	mm
Turns Per Coil	60	Units
Rotor outer diameter	1404.4	mm
Rotor inner diameter	1205	mm
Weights		
Stator core mass	2403.20	Kg
Total cooper mass	1137.71	Kg
<i>Total PM mass</i>	<i>743.42</i>	<i>Kg</i>
Rotor mass	2460.17	Kg
<i>Generator total mass</i>	<i>7702.03</i>	<i>Kg</i>
Costs		
Copper cost	11377.148	EUR
Lamination cost	120160.403	EUR
PM Cost	37171.42	EUR
Rotor Iron Cost	12300.88	EUR
Passive material cost	38510.19	EUR
Materials cost	219520.054	EUR
Energy loss cost	56260.65	EUR
<i>Total cost</i>	<i>275780.71</i>	<i>EUR</i>

Optimization Results for the 690V generator

The evolution of the genetic algorithm for the design of the 690V PMSG is shown in Figure 12.

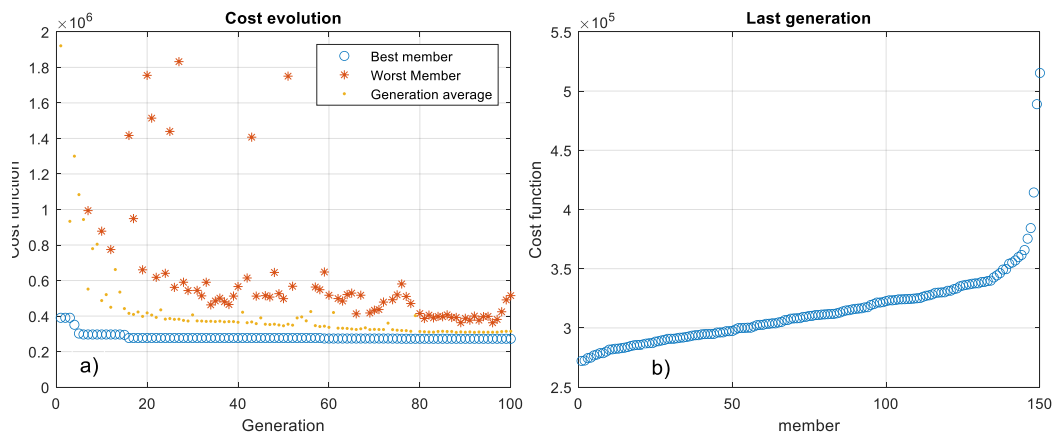


Figure 12 Evolution of the genetic algorithm for the 690V generator design. a) selected members from each generation. b) All the members of the last generation.

The evolution of the core design variables for the design of the 690V PMSG is shown in Figure 13.

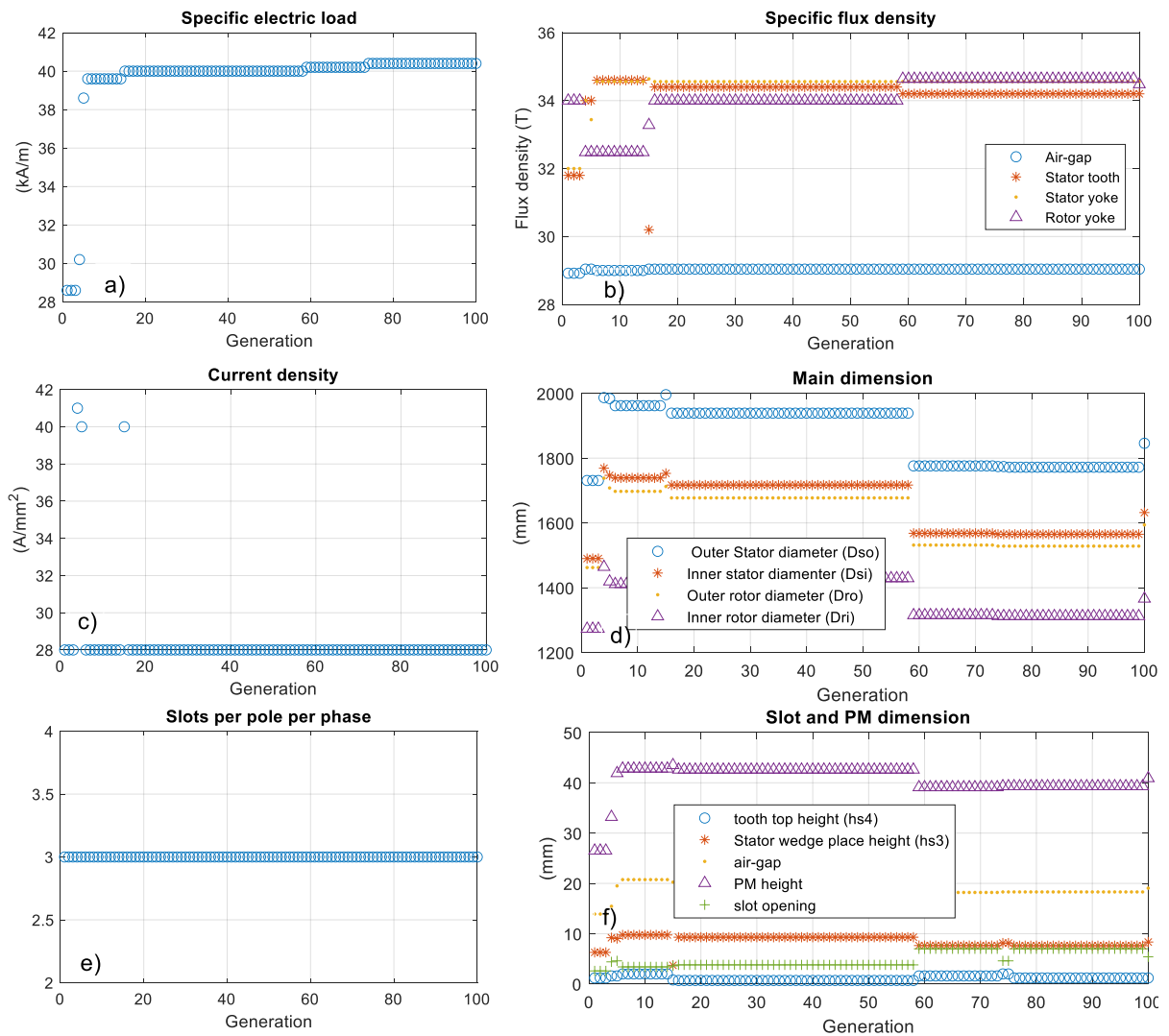


Figure 13 Evolution of design variables for the 690V generator a) Electric load b) Flux densities c) Current density d) Dimensions e) slots per pole per phase f) slot dimension

Figure 14 shows the evolution of the performance and cost-related variables of the 690V PMSG design.

Table XV list the values of the best member of the final generation of the genetic algorithm. These values are treated as the optimized and used for the design of the 690V PMSG.

Table XV Results of the genetic algorithm optimization for the 690V PMSG

Optimized Variable	Units	Optimized value
Linear electric loading, J_l	A/m	40.40e3
Airgap flux density, B_{ag}	Teslas	0.76
Stator teeth flux density, B_{st}	Teslas	2.05
Stator yoke flux density, B_{sy}	Teslas	2.12
Rotor yoke flux density, B_{ry}	Teslas	2.14
Stator current density, J_s	A/mm ²	3.60
Machine shape factor, or core stack length per pole pitch $\lambda_c = l_{stack}/\tau$	Units	1.5
Slots per pole per phase, q_1	Units	3
Slot opening, s_o	mm	5.4

Tooth top height, H_{s4}	mm	1.2
Coil span per pole pitch, y_1	Per unit	1
Embrace or Ratio of PM width to pole pitch α_m	Per unit	0.51

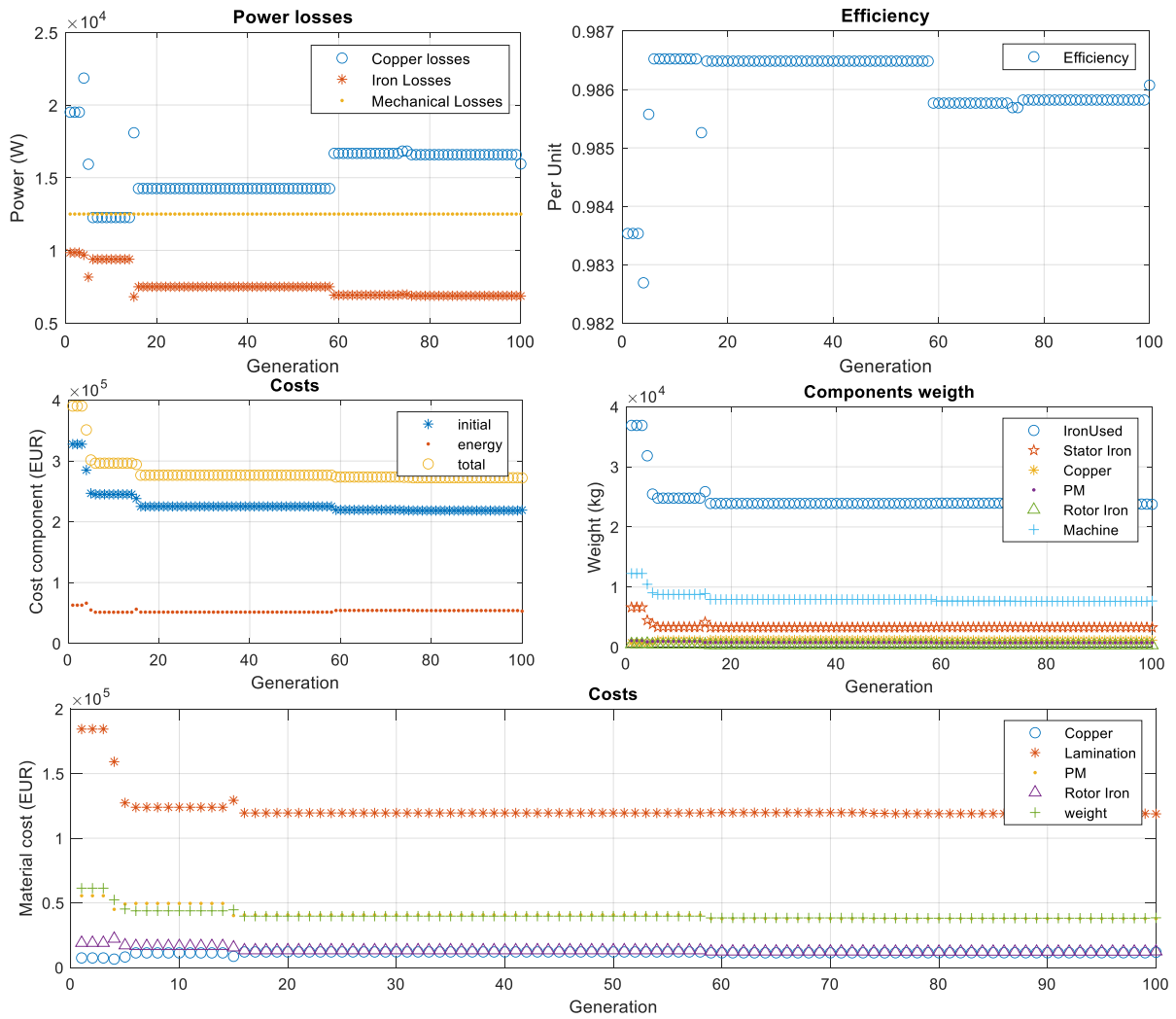


Figure 14 Performance and cost related variable evolution for a 690V generator a) power losses b)Efficiency c) Costs d) Weights e) Material costs

Table XIII list the results of using the optimized variables in the design process of the 690V PMSG, including the calculated efficiency, size, weight and cost.

Table XVI PMSG design parameters of the 2.5MW 690V using optimized variables

Design Parameter	Optimized Value	Units
Rated power	2.5e6	Watts
Rated Frequency	25	Hz
Rated Phase Voltage	398.37 (690/sqrt(3))	V
Iq rms current	2531.48	A
Rated copper loss	15947.4	W
Rated Iron loss	6860.9	W
Rated Mechanical Loss	12500	W
Rated Efficiency	0.98607	Per Unit
Constructive Dimensions		
Stator outer diameter	1846	mm

Stator inner diameter	1632	mm
Stator tooth pole tip height	1.2	mm
Stator wedge place height	8.33	mm
Overall slot height	34.59	mm
Stator yoke width	72.40	mm
Stator tooth width	26.39	mm
Air-gap height	19.05	mm
PM height	40.9	mm
Machine shape factor	1.5	Units
Stator coil height	24.4	mm
Stator slot width (root)	47.84	mm
Stator coil width (top)	45.71	mm
Stator slot mouth	5.4	mm
Radius of tooth head	825.5	mm
Turns Per Coil	12	Units
Rotor outer diameter	1593	mm
Rotor inner diameter	1366	mm
Weights		
Stator core mass	2376.36	Kg
Total cooper mass	1178.2	Kg
<i>Total PM mass</i>	<i>754.88</i>	<i>Kg</i>
Rotor mass	2481.5	Kg
<i>Generator total mass</i>	<i>7686.64</i>	<i>Kg</i>
Costs		
Copper cost	11782.51	EUR
Lamination cost	118818.00	EUR
PM Cost	37744.13	EUR
Rotor Iron Cost	12407.50	EUR
Passive material cost	38433.22	EUR
Materials cost	219185.38	EUR
Energy loss cost	52962.59	EUR
<i>Total cost</i>	<i>272147.98</i>	<i>EUR</i>

Finally, Table XVII shows a comparison of key optimized variables for each generator which are relevant or the final selection of best design based in the X-rotor requirements. As seen in the table, the optimized values for both designs are close in terms of efficiency and cost however, the 3.3KV PMSG generator has a smaller diameter and uses less permanent magnet material which could be beneficial for the design goals of the X-rotor system as discussed in section 3. Further design validations, using electromagnetic field solvers will also help to evaluate the advantages of each deployments in terms transient performance and magnetization. This is analysed in detail in the following section of the report.

Table XVII Comparison of key optimized variables for the 690V and 3.3KV PMSG designs

Optimized Variable	690V PMSG	3.3KV PMSG
<i>Rated Efficiency (PU)</i>	<i>0.986</i>	<i>0.9852</i>
<i>Stator outer diameter (mm)</i>	<i>1846</i>	<i>1633</i>
<i>Total PM mass (Kg)</i>	<i>754.88</i>	<i>743.42</i>
<i>Generator total mass (Kg)</i>	<i>7686.64</i>	<i>7702.03</i>
<i>Total cost (EUR)</i>	<i>272147.98</i>	<i>275780.71</i>

6. PMSG generator design validation using electromagnetic field solvers

3.3KV PMSG

Using the design parameters in Table XIV a 2D structure of the PMSG was generated using Ansys-Maxwell via RMXprt which is template-based electrical machine design tool that provides fast, analytical calculations of machine performance and 2-D and 3-D geometry creation for detailed finite element calculations in ANSYS Maxwell. RMXprt creates a high-fidelity, nonlinear equivalent circuit models, accounting for a machine's physical dimensions, winding characteristics, nonlinear material properties, and existing dynamic effects as eddy-currents.

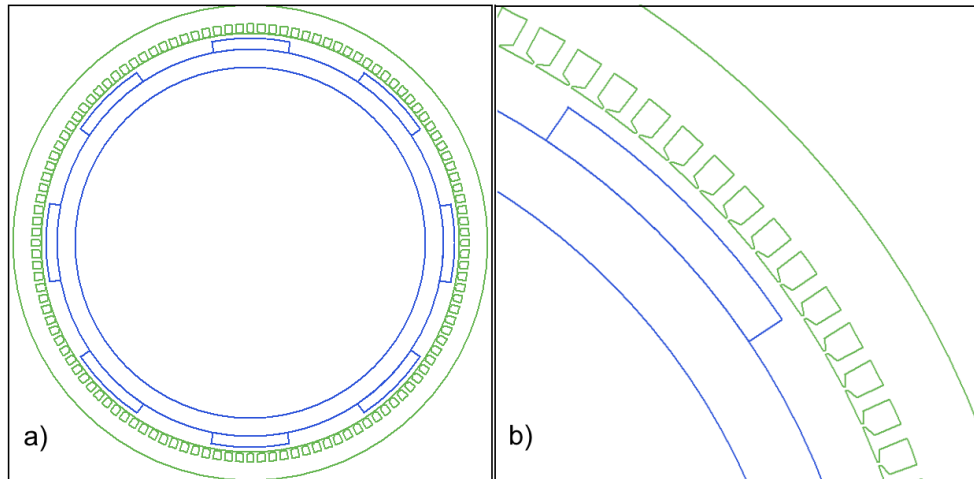


Figure 15 RMXprt design of the 3.3KV PMSG a) Full view b) zoomed view

Using the optimized variables in Table XIV as inputs, an analysis of the Full load operation conditions and no-load operation is computed using RMXprt. These evaluations are shown in Figure 16 and are useful to corroborate the calculations in the design procedure. As seen in Figure 16 a) The machine efficiency and air gap flux density are very close to the calculated values using the design procedure equations. RMXprt stator and rotor (teeth and yoke) flux densities results are lower than the calculated using the design procedure however, the flux values provided by RMXprt are obtained at no load operation. Later in the report, a full 2-D transient simulation will be carried out to visualize the intensities of the fluxes at full load.

Performance Design Sheet Curves				
Data: Full-Load Operation				
	Name	Value	Units	Description
1	RMS Line Current	455.94	A	
2	RMS Phase Current	455.94	A	
3	Armature Thermal Load	137.07	A ² /mm ³	
4	Specific Electric Loading	36333.4	A_per_meter	
5	Armature Current Density	3772570	A_per_m2	
6	Frictional and Windage Loss	12500	W	
7	Iron-Core Loss	0.21584	W	
8	Armature Copper Loss	40229	W	
9	Total Loss	40229	W	
10	Output Power	2.5003E+06	W	
11	Input Power	2.5406E+06	W	
12	Efficiency	98.4165	%	
13	Apparent Power	2661110	VA	
14	Power Factor	0.939583		
15	Synchronous Speed	375	rpm	
16	Rated Torque	64694.8	NewtonMeter	
17	Power Angle	20.5847	deg	
18	Maximum Output Power	6.9111E+06	W	
19	Short Circuit Current	1253.9	A	

a)

Performance Design Sheet Curves				
Data: No-Load Operation				
	Name	Value	Units	Description
1	Stator-Teeth Flux Density	1.87297	tesla	
2	Stator-Yoke Flux Density	1.50267	tesla	
3	Rotor-Yoke Flux Density	1.75663	tesla	
4	Air-Gap Flux Density	0.716548	tesla	
5	Magnet Flux Density	0.773461	tesla	
6	Stator-Teeth Ampere Turns	237.906	A.T	
7	Stator-Yoke Ampere Turns	503.407	A.T	
8	Rotor-Yoke Ampere Turns	850.181	A.T	
9	Air-Gap Ampere Turns	9793.63	A.T	
10	Magnet Ampere Turns	-11382.6	A.T	
11	Leakage-Flux Factor	1		
12	Stator Yoke Correction Factor	0.61648		Correction factor for stator yoke magnetic circuit length
13	Rotor Yoke Correction Factor	0.591157		Correction factor for rotor yoke magnetic circuit length
14	Fundamental Back emf	3246780	mV	
15	THD of Back emf	3.95205	%	
16	Cogging Torque	30.2541	NewtonMeter	

b)

Figure 16 RMXprt results for the design of a PMSG with the optimized variables of the 3.3KV PMSG a) Full load operation values, b) No load operation values.

Figure 17 shows several plots of the RMxprt-calculated coil voltages, currents, airgap flux density, induced voltages, efficiency and power of the 3.3KV PMSG.

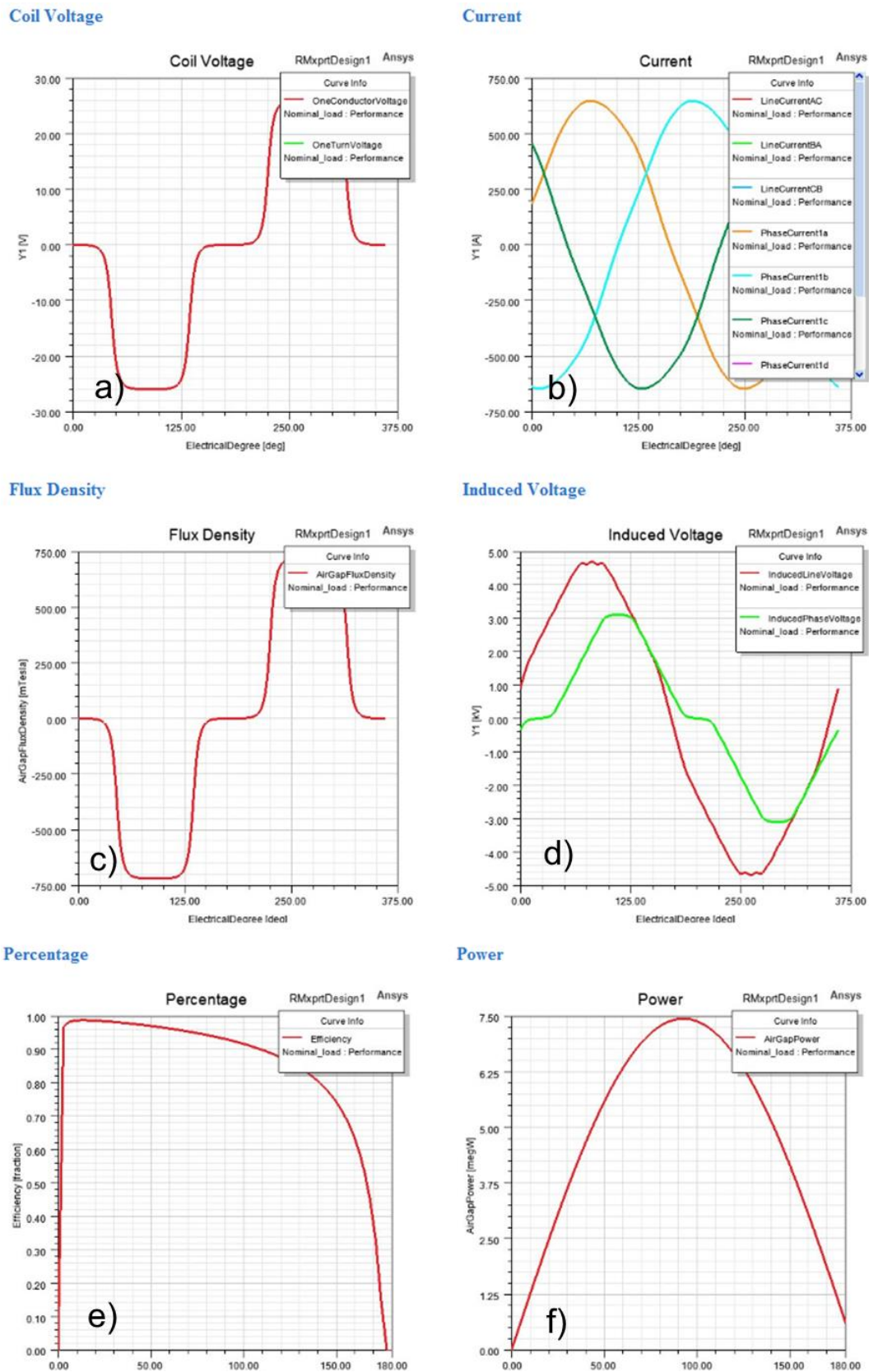


Figure 17 RMxprt-calculated values of the 3.3KV PMSG a) coil voltages b) currents, c) airgap flux density, d) induced voltages, e) efficiency f) power curve

Using the design parameters and materials of the 3.3KV PMSG a 2-D finite-element transient simulation was performed using Ansys-Maxwell to obtain the time expression of voltages currents and output power and flux densities at full load. The results of this simulations are shown in Figure 18 and Figure 19.

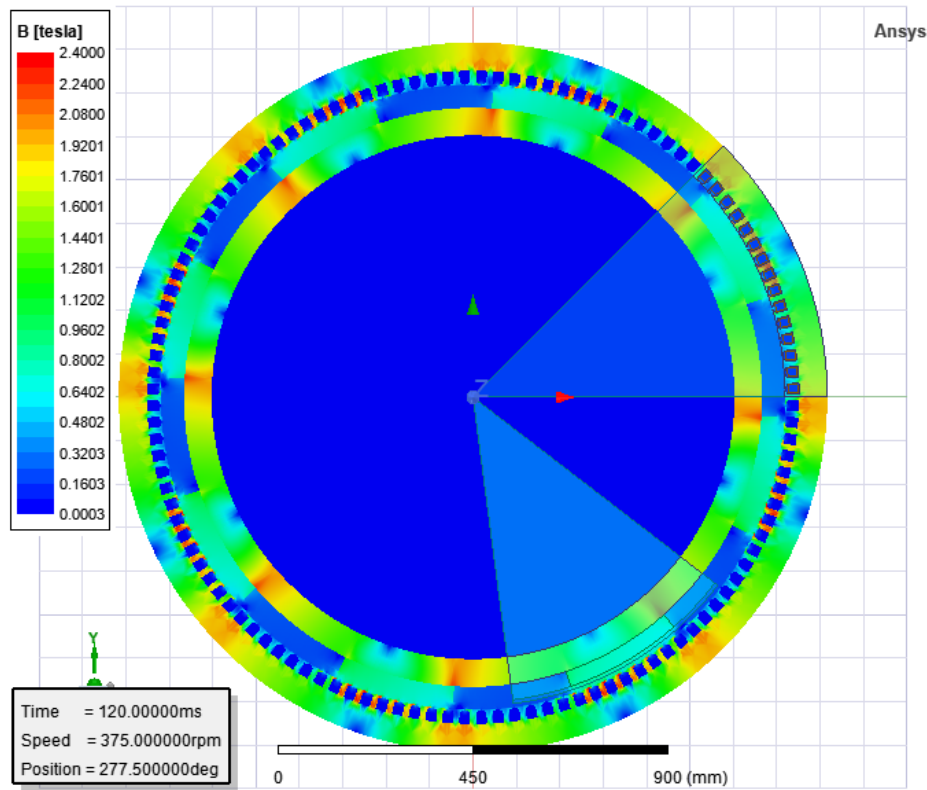


Figure 18 B-field magnitude for the 3.3KV PMSG at 120 ms.

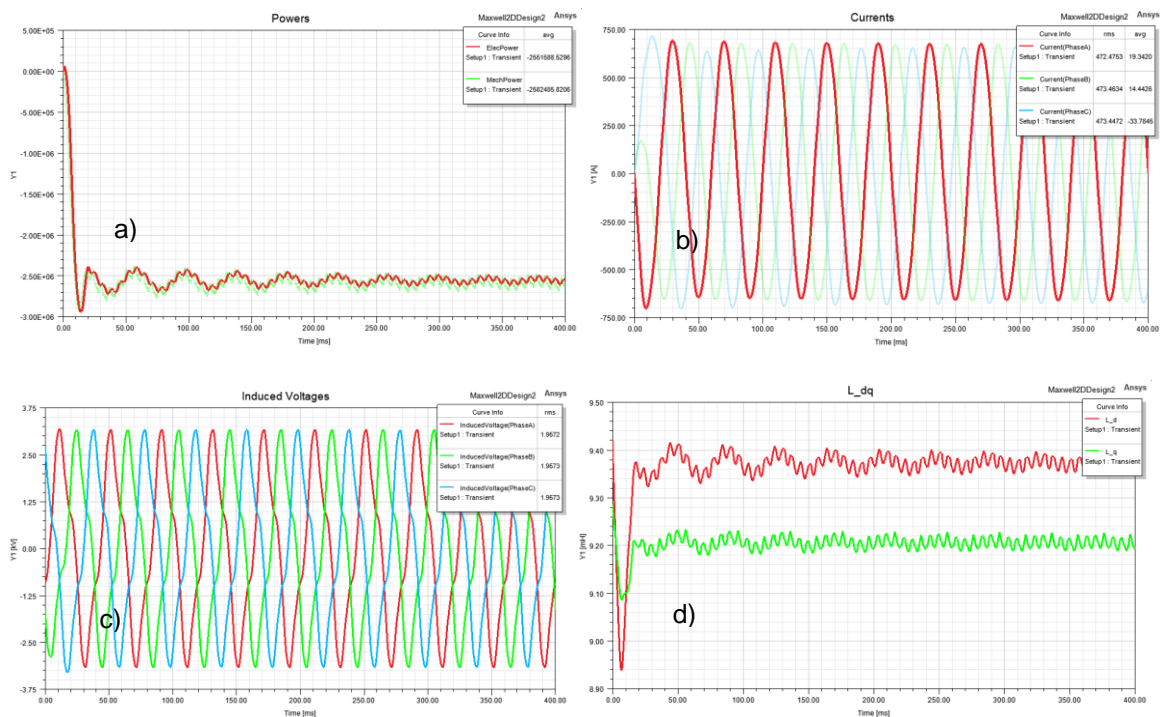


Figure 19 2-D finite-element transient simulation of the 3.3kv PMSG a) Torques, b) Currents c) Voltages, d) d-q inductances.

As seen in Figure 18 the maximum flux densities in the different sections of the PMSG structure are consistent with the optimized design parameters in Table XIII. Figure 19 2-D finite-element transient simulation of the 3.3kV PMSG a) Torques, b) Currents c) Voltages, d) d-q inductances. Figure 19 a) shows the transient torques of the machine evidencing the calculated efficiency of the energy conversion. Figure 19 2-D finite-element transient simulation of the 3.3kV PMSG a) Torques, b) Currents c) Voltages, d) d-q inductances. d) shows the transient values of the d and q inductances. Such values will be used to create an electrical simulation model of the machine.

690V PMSG

Using the design parameters in Table XVI a 2D structure of the PMSG was generated using Ansys-Maxwell via RMXprt as seen in Figure 20.

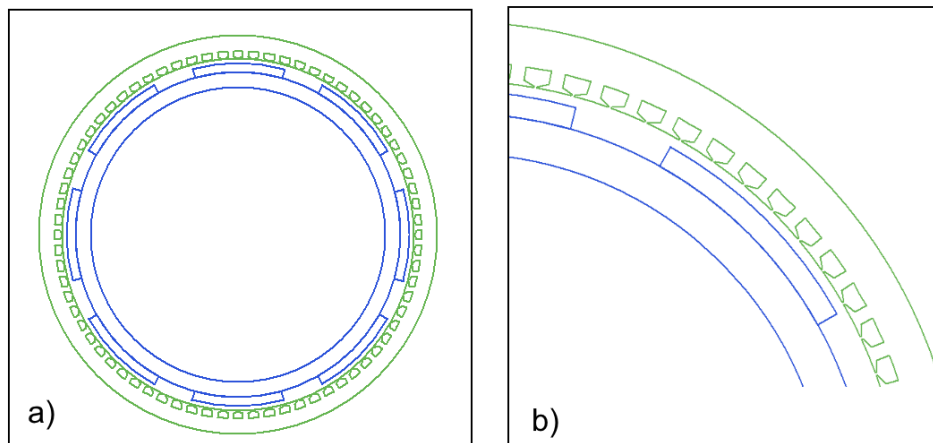


Figure 20 RMXprt design of the 690V PMSG a) Full view b) zoomed view

Using the optimized variables in as inputs, an analysis of the full load operation conditions and no-load operation is computed using RMXprt. These evaluations are shown in Figure 21 and are useful to corroborate the calculations in the design procedure. As seen in Figure 21 a) The machine efficiency and current density are close to the calculated values using the design procedure equations. In general RMXprt flux densities results are lower than the calculated using the design procedure however the flux values provided by RMXprt are obtained at no load operation. Later in the report, a full 2-D transient simulation will be carried out to visualize the intensities of the fluxes at full load.

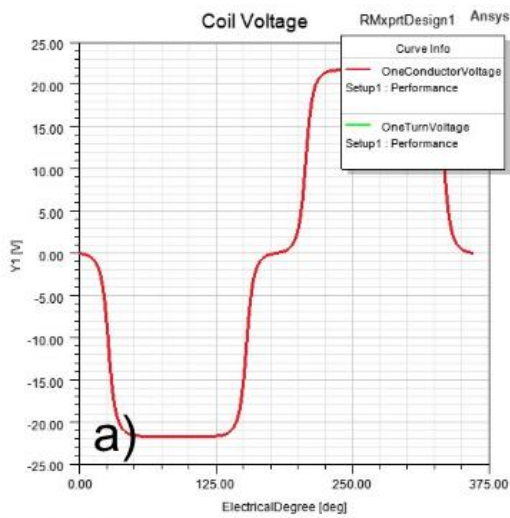
Name	Value	Units	Description
1 RMS Line Current	2112.8	A	
2 RMS Phase Current	2112.8	A	
3 Armature Thermal Load	100.992	A ² /mm ³	
4 Specific Electric Loading	29.671	kA_per_meter	
5 Armature Current Density	3403790	A_per_m2	
6 Frictional and Windage Loss	12500	W	
7 Iron-Core Loss	0.35775	W	
8 Armature Copper Loss	10357	W	
9 Total Loss	35357	W	
10 Output Power	2.5003E+06	W	
11 Input Power	2.5356E+06	W	
12 Efficiency	98.6056	%	
13 Apparent Power	2527670	VA	
14 Power Factor	0.989153		
15 Synchronous Speed	375	rpm	
16 Rated Torque	64568.8	NewtonMeter	
17 Power Angle	14.961	deg	
18 Maximum Output Power	9.579E+06	W	
19 Short Circuit Current	9186.4	A	

Name	Value	Units	Description
1 Stator-Teeth Flux Density	1.68124	tesla	
2 Stator-Yoke Flux Density	1.91782	tesla	
3 Rotor-Yoke Flux Density	2.54896	tesla	
4 Air-Gap Flux Density	0.737765	tesla	
5 Magnet Flux Density	0.807152	tesla	
6 Stator-Teeth Ampere Turns	11.0555	A.T	
7 Stator-Yoke Ampere Turns	101.862	A.T	
8 Rotor-Yoke Ampere Turns	109.829	A.T	
9 Air-Gap Ampere Turns	11702.2	A.T	
10 Magnet Ampere Turns	-11925.8	A.T	
11 Leakage-Flux Factor	1		
12 Stator Yoke Correction Factor	0.766794		Correction factor for stator yoke magnetic circuit length
13 Rotor Yoke Correction Factor	0.766794		Correction factor for rotor yoke magnetic circuit length
14 Fundamental Back emf	752183	mV	
15 THD of Back emf	3.9965	%	
16 Cogging Torque	82.3938	NewtonMeter	

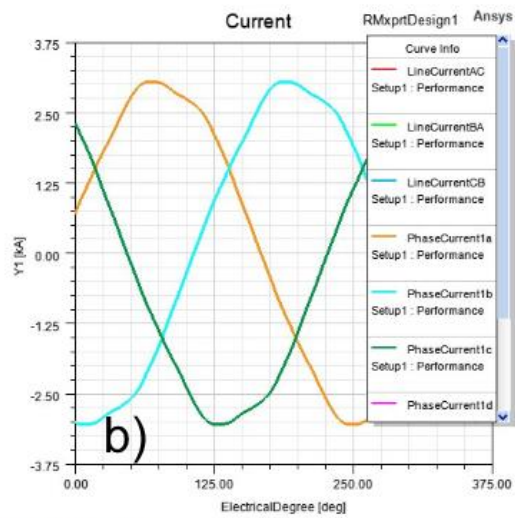
Figure 21 RMXprt results for the design of a PMSG with the optimized variables of the 690V PMSG a) Full load operation values, b) No load operation values.

Figure 22 shows several plots of the RMxprt-calculated coil voltages, currents, airgap flux density, induced voltages, efficiency and power of the 690V PMSG.

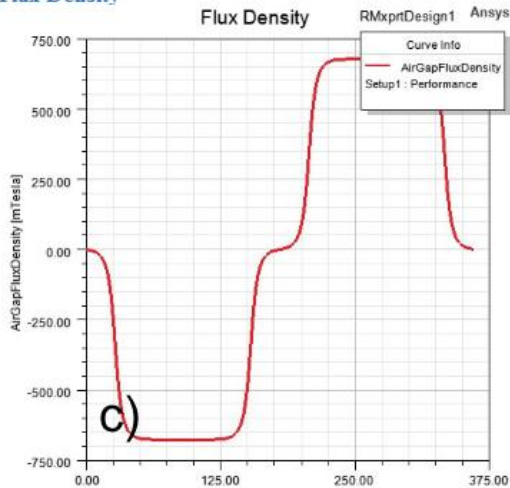
Coil Voltage



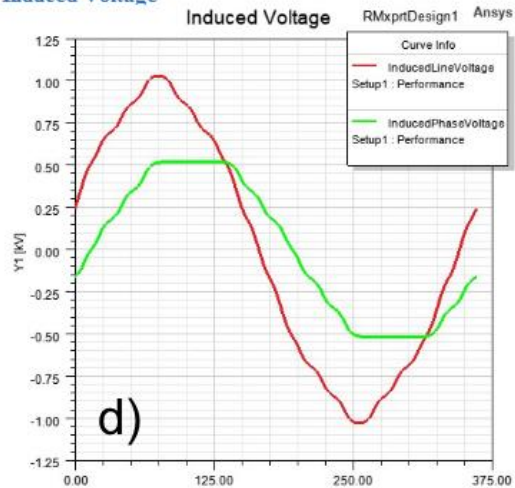
Current



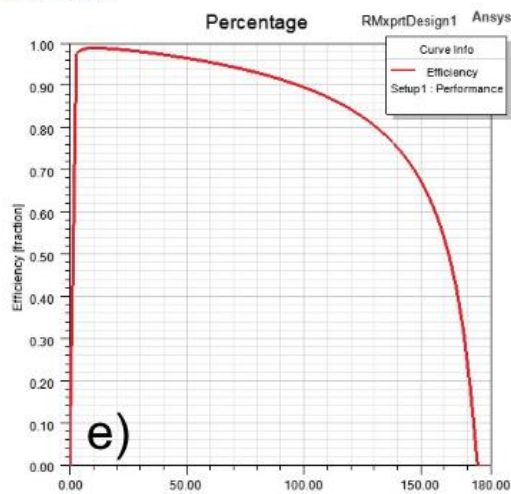
Flux Density



Induced Voltage



Percentage



Power

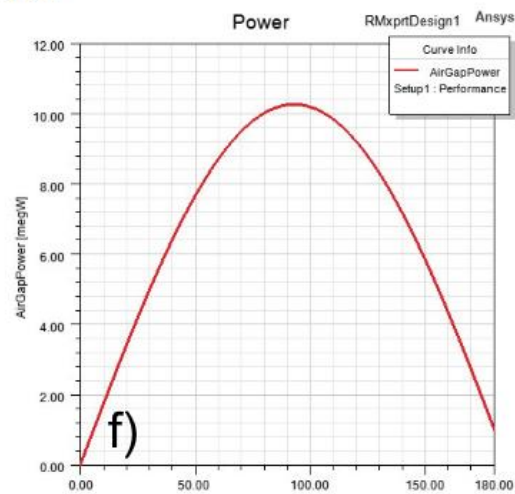


Figure 22 RMxprt-calculated values of the 690V PMSG a) coil voltages b) currents, c) airgap flux density, d) induced voltages, e) efficiency f) power curve

Using the design parameters and materials of the 690V PMSG a 2-D finite-element transient simulation was performed using Ansys-Maxwell to obtain the time expression of voltages currents and output power and flux densities at full load. The results of this simulations are shown in Figure 23 and Figure 24.

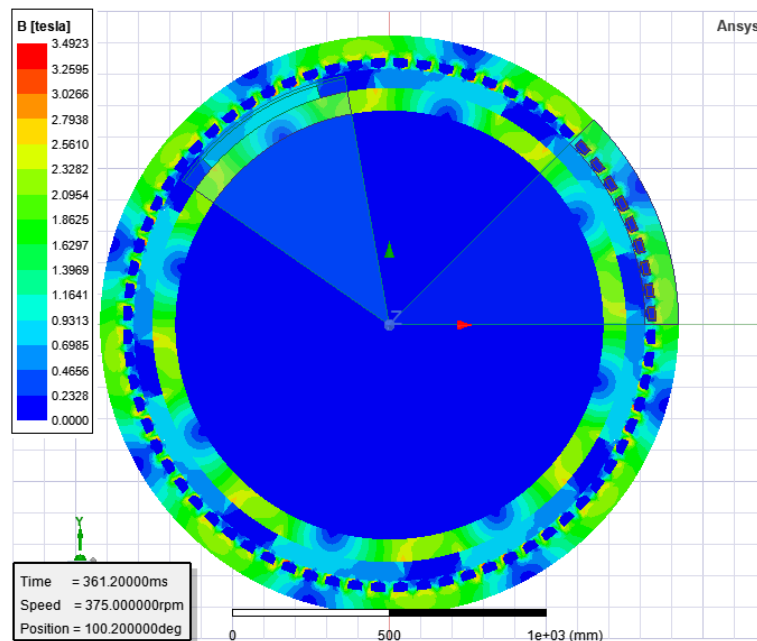


Figure 23 B-field magnitude for the 690V PMSG at 361 ms.

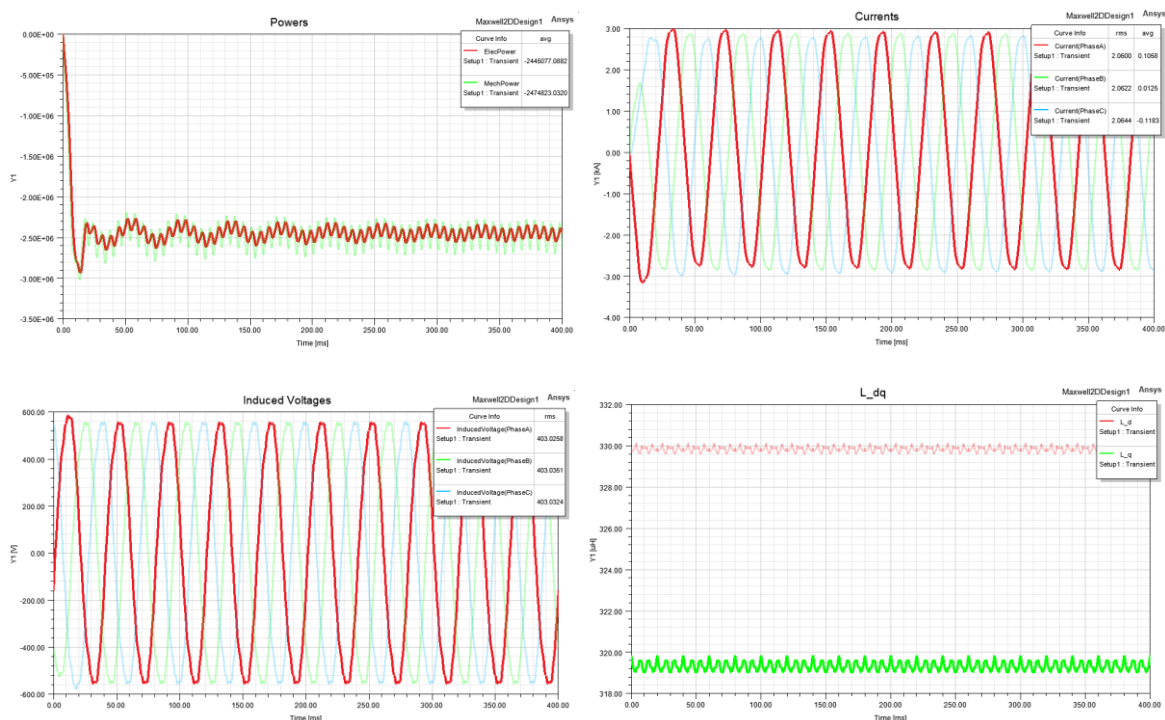


Figure 24 2-D finite-element transient simulation of the 690V PMSG a) Torques, b) Currents c) Voltages, d) d-q inductances.

As seen in Figure 23 and Figure 24 the 690V PMSG suffers from some points of excessive magnetic strength which were not accounted in the design procedure. Those are larger than for the case of the

3.3KV generator. Additionally the 690V generator shows larger torque ripple due to the presence of higher harmonic distortion in both voltage and current values.

7. Analysis of power electronic requirements using electrical modelling and simulations

Using the inductance, resistance and Flux Linkages parameters calculated by RMxprt for each machine an electrical stimulation of the performance of the generator was carried out using Simulink.

The developed Simulink model connects the PMSG to a back to back power electronic converter controlling its rotational speed. The control system of the back to back converter commands the machine to increase its rotational speed from 1 PU (375 RPM) to 1.5 PU (562.5 RPM), which is consisted with some of the operational strategies for the X-rotor presented in section 2. The Simulink model uses a 2-level, 1200 VDC power electronic interface for the 690V PMSG and a three-level 5.3KV power electronic interface for the 3.3KV PMSG as indicated by Table IV.

The electrical parameters for the simulation of the PMSGs are presented in Table XVIII.

Table XVIII Electrical parameters used for the simulation of the PMSGs

Simulation parameter	690V	3.3KV
Number of phases	3	3
Back EMF waveform	Sinusoidal	Sinusoidal
Rotor type	Round	Round
Mechanical Input	Torque	Torque
Stator Phase resistance	.00170675	0.04446
Armature Inductance	0.33973e-3	10.048e-3
Flux Linkages established by Magnets	2.6014	12.0604
Pole Pairs	4	4
Inertia constant	0.5s	0.5s

A picture of the developed model in Simulink is shown in Figure 25 and a schematic diagram of the speed control structure is shown in Figure 26.

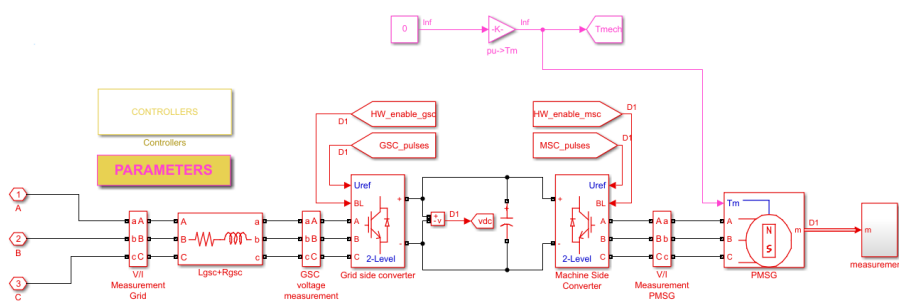


Figure 25 Simulink Model to evaluate the power electronic requirements of the PMSG

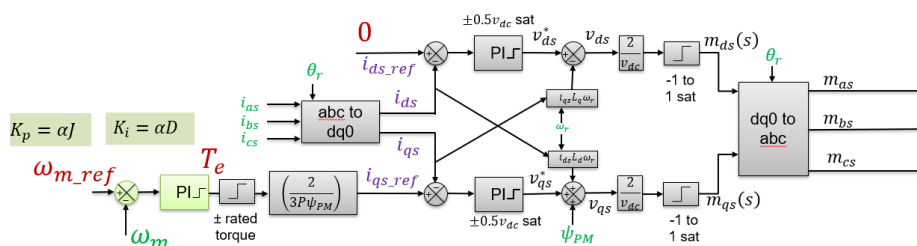


Figure 26 Rotor speed controller implemented in the grid side converter of Simulink model.

Electrical simulation results of the 690V PMSG

The simulation seeks to evaluate the control capabilities of the power electronic converter for overspeed operation of the PMSG. When the generator overspeed, the level of the voltage at its terminals increases. When this happens the power electronic converter needs to increase its output voltage to maintain proper control over the currents circulating between the generator and the converter. The control structure uses the I_q current to control the speed of the machine (via electromagnetic torque manipulation) and the I_d current is kept in 0 to have a linear relationship between torque and I_q current. The current control capabilities of the power electronic converter are limited by the maximum voltage it can reproduce at its terminals. Which can reach a maximum of half the DC bus voltage (i.e. 600 VAC peak for a 1200 VDC bus). When the phase voltage at the terminals of the generator reach a magnitude of 600VAC the power electronic converter is no longer capable to control the variables of the machine unless the DC bus voltage is increased. However, as described in section 4, increasing the DC bus voltage adversely affects the efficiency and reliability of the power electronic converter.

Figure 27 show a speed control simulation from 1 to 1.5 PU speed at steps of 0.1 every 5 seconds for a 690V phase to phase PMSG with 0 PU mechanical torque input (i.e. no load). From the period from 0 to 5 seconds Figure 27 a) and c) shows that the initial no-load peak magnitude of the PMSG phase voltage at 1 PU speed is of around 400V. Figure 27 e) shows that both the mechanical and output power of the generator are 0 and Figure 27 d) and f) show that both d and q current are kept at their specific reference. Form 5 second onward the speed of the machine increases in steps of 0.1 PU every 5 seconds. Each increment produces an increase in the generator voltages as seen in Figure 27 a) and c). The increases of speed in the machine are created by modifying momentarily the electromagnetic torque of the machine, via I_q current control. In second 24 the speed is already at 1.4 PU and the voltage of the PMSG is very close to half of the DC bus voltage. When the machine tries to reach 1.5 PU speed at second 25 the machine voltage is locked to the maximum power electronic voltage and the control of I_d and I_q current is lost. This is evident in Figure 27 d) and f) after 25 seconds. Since current control is lost, there is no longer control over the speed of the generator which begins to fluctuate. This evidences that Under no load conditions, the maximum overspeed allowed for the 690V PMSG is 1.48 PU if the converter uses a DC bus of 1200 VDC.

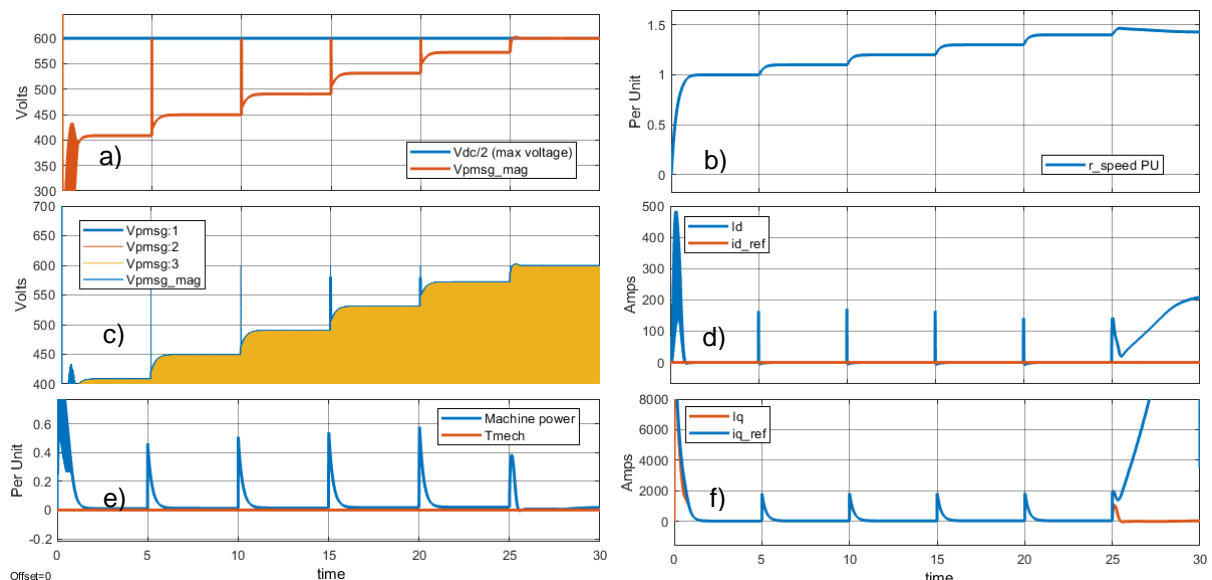


Figure 27 No-load simulation of the 690V PMSG for different speeds a) Voltage Magnitude b) Machine speed c) 3 Phase Voltages d) I_d current e) I_q current.

Figure 28 show a speed control simulation from 1 to 1.5 PU speed at steps of 0.1 every 5 seconds for a 690V phase to phase PMSG with -1 PU mechanical torque input (i.e. full generator load). From the period from 0 to 5 seconds Figure 28 a) and c) shows that the initial full-load peak magnitude of the

PMSG phase voltage at 1 PU speed is of around 450V (50V higher than no load condition). Figure 28 e) shows that both the mechanical and output power of the generator are -1 and Figure 28 d) and f) show that both d and q current are kept at their specific reference. From 5 second onward the speed of the machine increases in steps of 0.1 PU every 5 seconds. Each increment produces an increase in the generator voltages as seen in Figure 28 a) and c). The increases of speed in the machine are created by modifying momentarily the electromagnetic torque of the machine, via I_q current control. In second 19 the speed is already at 1.3 PU and the voltage of the PMSG is very close to half of the DC bus voltage. When the machine tries to reach 1.4 PU speed at second 20 the machine voltage is locked to the maximum power electronic voltage and the control of I_d and I_q current is lost. This is evident in Figure 28 d) and f) after 20 seconds. Since current control is lost, there is very little control over currents of the generator, and even though the I_q current control manages to keep the speed at the desired value, the I_d current is no longer kept at 0, meaning an increase of reactive currents in the machine circuit and current overload for the power electronic converter. This evidences that Under full load conditions, the maximum overspeed allowed for the 690V PMSG is 1.28 PU if the converter uses a DC bus of 1200 VDC.

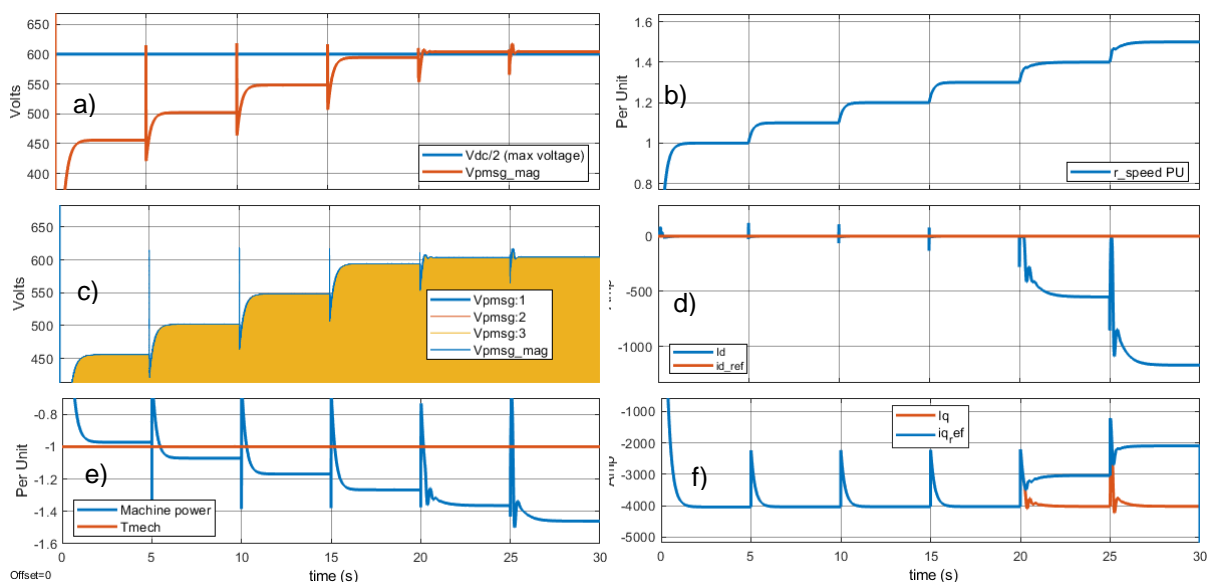


Figure 28 full-load simulation of the 690V PMSG for different speeds a) Voltage Magnitude b) Machine speed c) 3 Phase Voltages d) I_d current e) I_q current.

Electrical simulation results of the 3.3KV PMSG

Figure 29 show a speed control simulation from 1 to 1.5 PU speed at steps of 0.1 every 5 seconds for the 3.3KV phase to phase PMSG with 0 PU mechanical torque input (i.e. no load). From the period from 0 to 5 seconds Figure 29 a) and c) shows that the initial no-load peak magnitude of the PMSG phase voltage at 1 PU speed is of around 1900V. Figure 29 e) shows that both the mechanical and output power of the generator are 0 and Figure 29 d) and f) show that both d and q current are kept at their specific reference. From 5 second onward the speed of the machine increases in steps of 0.1 PU every 5 seconds. Each increment produces an increase in the generator voltages as seen in Figure 29 a) and c). The increases of speed in the machine are created by modifying momentarily the electromagnetic torque of the machine, via I_q current control. In second 19 the speed is already at 1.3 PU and the voltage of the PMSG is very close to half of the DC bus voltage (i.e 2650VDC). When the machine tries to reach 1.4 PU speed at second 20 the machine voltage is locked to the maximum power electronic voltage and the control of I_d and I_q current is lost. This is evident in Figure 27 d) and f) after 20 seconds. Since current control is lost, there is no longer control over the speed of the generator which begins to fluctuate. This evidences that under no load conditions, the maximum overspeed allowed for the 3.3KV PMSG is 1.38 PU if the converter uses a DC bus of 5.3 KVDC.

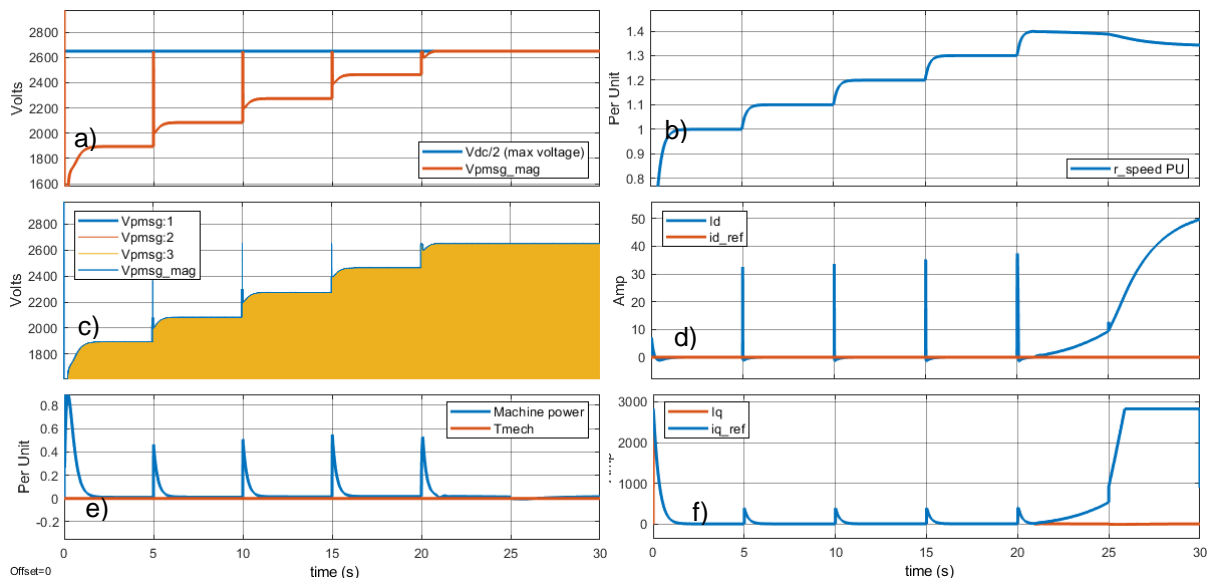


Figure 29 no-load simulation of the 3.3KV PMSG for different speeds a) Voltage Magnitude b) Machine speed c) 3 Phase Voltages d) Id current e) Iq current.

Figure 30 show a speed control simulation from 1 to 1.5 PU speed at steps of 0.1 every 5 seconds for a 3.3KV phase to phase PMSG with -1 PU mechanical torque input (i.e. full generator load).

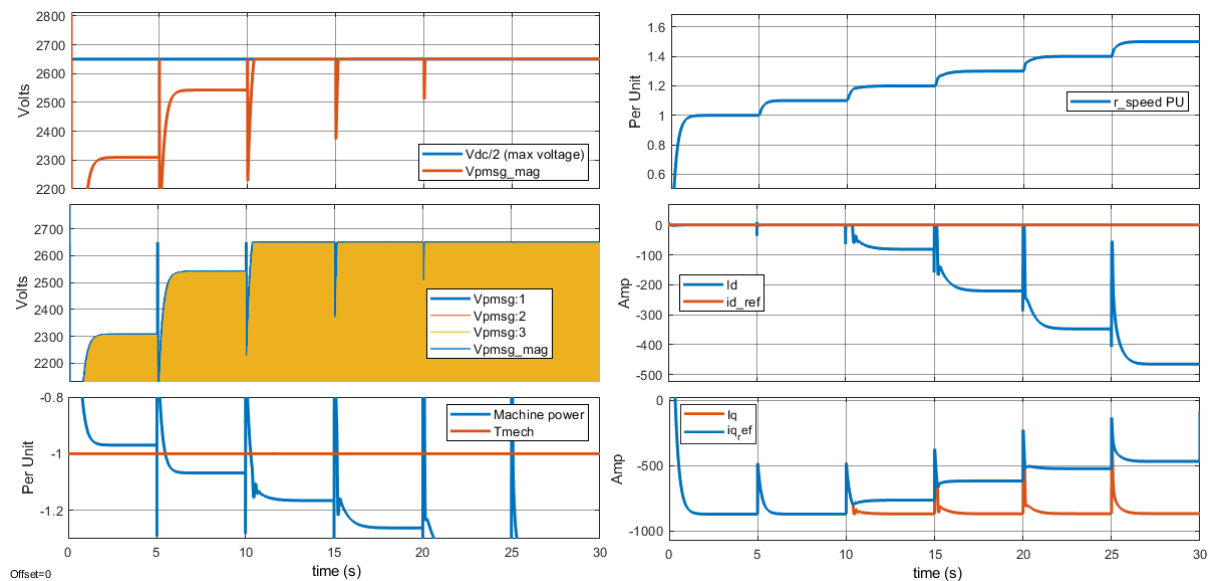


Figure 30 full-load simulation of the 3.3KV PMSG for different speeds a) Voltage Magnitude b) Machine speed c) 3 Phase Voltages d) Id current e) Iq current.

From the period from 0 to 5 seconds Figure 30 a) and c) shows that the initial full-load peak magnitude of the PMSG phase voltage at 1 PU speed is of around 2300V (400V higher than no load condition). Figure 30 e) shows that both the mechanical and output power of the generator are -1 and Figure 30 d) and f) show that both d and q current are kept at their specific reference. From 5 second onward the speed of the machine increases in steps of 0.1 PU every 5 seconds. Each increment produces an increase in the generator voltages as seen in Figure 30 a) and c). The increases of speed in the machine are created by modifying momentarily the electromagnetic torque of the machine, via Iq current control. In second 9 the speed is already at 1.1 PU and the voltage of the PMSG is very close to half of the DC bus voltage. When the machine tries to reach 1.2 PU speed at second 10 the machine voltage is locked

to the maximum power electronic voltage and the control of I_d and I_q current is lost. This is evident in Figure 30 d) and f) after 10 seconds. Since current control is lost, there is very little control over currents of the generator, and even though the I_q current control manages to keep the speed at the desired value, the I_d current is no longer kept at 0, meaning an increase of reactive currents in the machine circuit and current overload of the power electronic converter, such an overload would produce a power imbalance between converters making the DC voltage to increase into destructive levels. This evidences that Under full load conditions, the maximum overspeed allowed for the 3.3KV PMSG is 1.15 PU if the converter uses a DC bus of 5300 VDC.

8. Summary of deliverable outcomes

This deliverable has presented a detailed analysis of the optimal design of PMSG for the X-rotor seeking to comply with the operation strategy of the system, structural limitations and operational ranges. The results of this deliverable include up-to-date information of industrial practices for the development and control of PMSG for wind turbine applications. This information provides light in the practices and maturity of different wind generator development strategies and sets the path to follow to develop a commercially doable system.

With regards to the design of the PMSG system, the deliverable applies an authoritative design methodology aided by an optimization algorithm and real manufacture constraints to develop an optimal design for a 690V and 3.3KV PMSG machines, since both options could be suitable for the X-rotor system. The optimal design are validated using 2D models and finite element analysis. A detailed list of design variables are provided for each case, including relevant information to realize the objectives of the X-rotor project, (such as efficiency, weight, cost, and size).

Finally this deliverable analyses the electric performance of the designed machines under operation conditions that mimic the most extreme operation strategies of the X-rotor. This analysis is used to asses the adequacy of commercial power converters to exert control under those conditions. Clear limits have been identified and presented to the designers for each generator design case.

9. Conclusions

There exists a trade-off between the selection the voltage level of the PMSG for the X-rotor. In one hand low voltage generators and their associated power electronics enable longer control range which is beneficial for some operation strategies of the X-rotor. However they are larger in diameter and require more PM materials and larger transformer, cables and filters. In the other hand medium voltage generators are smaller in diameter and require less PM material, as well as smaller passive elements (such as transformers and cables) also, they have less torque ripple and cost. However this come with the penalty of less redundancy (for the power electronic converters) and lesser degree of control range, which limits the extent of the operation strategies of the X-rotor system. It seem, however that it is possible to increase the DC voltage level of medium voltage converters as seen in some commercial deployments. If this increase is possible and does not affect the reliability and power losses of medium voltage converters, then it can be concluded that a medium voltage generator with 3-level power electronic converter, as the once analysed in detail in this report, could be the most suitable option for the Rotor concept.

10. References

- [1] L. Morgan, " Control system development for the X-Rotor Wind Turbine -2nd Year Report," University of Strathclyde, 2021.
- [2] W. Leithead, A. Camciuc, A. K. Amiri, and J. Carroll, "The X-Rotor Offshore Wind Turbine Concept," *Journal of Physics: Conference Series*, vol. 1356, no. 1, p. 012031, 2019/10/01 2019, doi: 10.1088/1742-6596/1356/1/012031.
- [3] P. ALVES DIAS, S. BOBBA, S. CARRARA, and B. PLAZZOTTA, "THE ROLE OF RARE EARTH ELEMENTS IN WIND ENERGY AND ELECTRIC MOBILITY," 2020.

- [4] V. Yaramasu and B. Wu, "Predictive Control of a Three-Level Boost Converter and an NPC Inverter for High-Power PMSG-Based Medium Voltage Wind Energy Conversion Systems," *IEEE Transactions on Power Electronics*, vol. 29, no. 10, pp. 5308-5322, 2014, doi: 10.1109/TPEL.2013.2292068.
- [5] *ANSI C84.1-2011*, A. N. S. Institute, 2011.
- [6] *IEC 60038*, I. E. COMMISSION, 2009.
- [7] V. Yaramasu, B. Wu, P. C. Sen, S. Kouro, and M. Narimani, "High-power wind energy conversion systems: State-of-the-art and emerging technologies," *Proceedings of the IEEE*, vol. 103, no. 5, pp. 740-788, 2015, doi: 10.1109/JPROC.2014.2378692.
- [8] B. Wu, Y. Lang, N. Zargari, and S. Kouro, *Power Conversion and Control of Wind Energy Systems*. Wiley, 2011.
- [9] X. Yuanye, K. H. Ahmed, and B. W. Williams, "Different torque ripple reduction methods for wind energy conversion systems using diode rectifier and boost converter," in *2011 IEEE International Electric Machines & Drives Conference (IEMDC)*, 15-18 May 2011 2011, pp. 729-734, doi: 10.1109/IEMDC.2011.5994902.
- [10] W. Erdman and M. Behnke, "Low Wind Speed Turbine Project Phase II: The Application of Medium-Voltage Electrical Apparatus to the Class of Variable Speed Multi-Megawatt Low Wind Speed Turbines " National Renewable Energy Laboratory 2005.
- [11] R. Erickson, S. Angkititrakul, O. Al-Naseem, and G. Lujan, "Novel Power Electronics Systems for Wind Energy Applications: Final Report " National Renewable Energy Laboratory, Boulder, Colorado 2002.
- [12] L. Sethuraman and K. Dykes, "GeneratorSE: A Sizing Tool for Variable-Speed Wind Turbine Generators," National Renewable Energy Laboratory, 2017.
- [13] A. Hebala, W. A. M. Ghoneim, and H. A. Ashour, "Detailed Design Procedures for PMSG Direct-Driven by Wind Turbines," *Journal of Electrical Engineering & Technology*, vol. 14, no. 1, pp. 251-263, 2019/01/01 2019, doi: 10.1007/s42835-018-00010-y.
- [14] I. Boldea and L. Tutelea, *Electric Machines: Transients, Control Principles, Finite Element Analysis and Optimal Design with MATLAB*. CRC Press, 2021.
- [15] A. S. McDonald, "Structural Analysis of Low Speed, High Torque Electrical Generators for Direct Drive Renewable Energy Converters," PhD, The University of Edinburgh 2008.
- [16] P. E. Morthorst and L. Kitzing, "2 - Economics of building and operating offshore wind farms," in *Offshore Wind Farms*, C. Ng and L. Ran Eds.: Woodhead Publishing, 2016, pp. 9-27.
- [17] X.-S. Yang, "Chapter 6 - Genetic Algorithms," in *Nature-Inspired Optimization Algorithms (Second Edition)*, X.-S. Yang Ed.: Academic Press, 2021, pp. 91-100.
- [18] vacuumschmelze. <https://vacuumschmelze.com/products/Permanent-Magnets/NdFeB-Magnets---VACODYM> (accessed 2021).